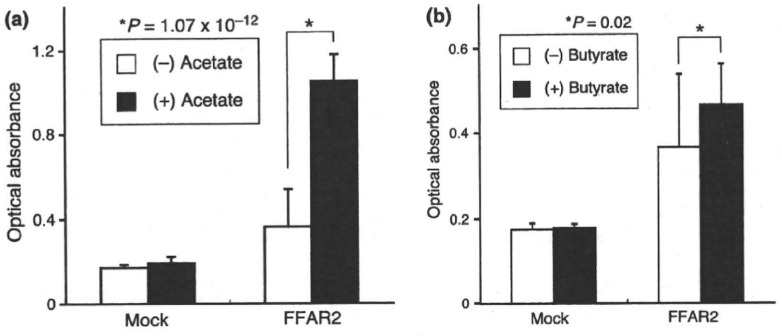

Fig. 5. Effect of short chain fatty acids on the proliferation of cells expressing free fatty acid receptor 2 (FFAR2). Mouse 3T3 cells infected with a virus encoding FFAR2 or with the empty virus (Mock) were cultured for 48 h in DMEM-F12 medium supplemented with 1% charcoal-treated fetal bovine serum in the absence or presence of (a) 100 mM sodium acetate or (b) 1 mM sodium butyrate. Cell proliferation was then assayed with the use of the WST-1 reagent. Data are expressed as absorbance at 450 nm and are means + SD of values from three independent experiments. *P*-values for the indicated comparisons were determined by Student's *t*-test.

ach.[16] In addition, FFAR2 has been detected in enterocytes of the rat intestine[18] as well as in those of the human colon.[19] The preferential expression of FFAR2 in the digestive tract and the mitogenic activity of the encoded protein together suggest a possible role for FFAR2 in carcinogenesis of the digestive system.

In our current analyses, both mRNA and protein amounts for *FFAR2* were frequently induced among the specimens for digestive tract cancer. However, DNA quantitation of the *FFAR2* locus failed to detect copy number changes of the genome (data not shown), and there are no CpG islands mapped closely or within the *FFAR2* locus in the human genome. Therefore, the molecular mechanism underlying such *FFAR2* induction is yet to be revealed.

SCFA, such as acetate, propionate, and butyrate, are the major products of the breakdown of dietary fiber by bacterial fermentation in the mammalian small and large intestine.[20] Among various SCFA, acetate has the highest selectivity for FFAR2.[21] The composition of SCFA in the colonic lumen is ~60% acetate, ~20% propionate, and ~20% butyrate.[22] SCFA are the major anions, being present at a total concentration of ~100 mM, in the lumen of the large intestine in mammals.[23] We found that the mitogenic effect of acetate in 3T3 cells expressing FFAR2 was maximal at ~100 mM (data not shown). These data suggest that FFAR2 may induce mitogenesis in the digestive tract in a manner dependent on the content of SCFA (especially that of acetate) in the diet.

It should be noted that a mere overexpression of FFAR2 significantly induced the growth of 3T3 cells even without the SCFA stimulation (Fig. 5). Although this observation potentially indicates a novel, SCFA-independent function of FFAR2, overexpression of cell surface receptors often stimulates their intracellular signaling with suboptimal concentrations of cognate ligands. Therefore, it is also possible that highly abundant FFAR2 proteins have evoked a mitogenic signaling in 3T3 in response to a low level of SCFA in the serum (or even independent of SCFA).

Diet has a substantial impact on the occurrence of digestive tract cancers, including GBC, gastric cancer, and CRC,[24] as well as on that of chronic inflammatory bowel diseases.[25] Our present findings suggest a possible connection between such disorders and either continuous exposure to SCFA in certain types of diet or induced expression of FFAR2 in the digestive tract. FFAR2 is thus a potential therapeutic target for these disorders.

Acknowledgments

We thank K. Sasaki for technical assistance and T. Kitamura (Institute of Medical Science, University of Tokyo) for the pMXS retroviral plasmid. This study was supported in part by Grants-in-Aid for Scientific Research from the Ministry of Education, Culture, Sports, Science, and Technology, Japan, and by grants from the Japan Society for the Promotion of Science, and from the Ministry of Health, Labour, and Welfare, Japan. The nucleotide sequence of the *FFAR2* cDNA isolated in this study has been deposited in DDBJ/GenBank under the accession number AB378083.

Abbreviations

ALK	anaplastic lymphoma kinase
EML4	echinoderm microtubule associated protein like-4
ERBB2	v-erb-b2 avian erythroblastic leukemia viral oncogene homolog 2
KRAS	v-ki-ras2 Kirsten rat sarcoma viral oncogene homolog
TP53	tumor protein p53

References

1 Carriaga MT, Henson DE. Liver, gallbladder, extrahepatic bile ducts, and pancreas. *Cancer* 1995; **75**: 171–90.
2 Cubertafond P, Gainant A, Cucchiaro G. Surgical treatment of 724 carcinomas of the gallbladder. Results of the French Surgical Association Survey. *Ann Surg* 1994; **219**: 275–80.
3 Jemal A, Siegel R, Ward E, Murray T, Xu J, Thun MJ. Cancer statistics, 2007. *CA Cancer J Clin* 2007; **57**: 43–66.
4 Zatonski WA, Lowenfels AB, Boyle P *et al.* Epidemiologic aspects of gallbladder cancer: a case–control study of the SEARCH Program of the International Agency for Research on Cancer. *J Natl Cancer Inst* 1997; **89**: 1132–8.
5 Hasumi A, Matsui H, Sugioka A *et al.* Precancerous conditions of biliary tract cancer in patients with pancreaticobiliary maljunction: reappraisal of nationwide survey in Japan. *J Hepatobiliary Pancreat Surg* 2000; **7**: 551–5.
6 Goldfarb M, Shimizu K, Perucho M, Wigler M. Isolation and preliminary characterization of a human transforming gene from T24 bladder carcinoma cells. *Nature* 1982; **296**: 404–9.
7 Soda M, Choi YL, Enomoto M *et al.* Identification of the transforming *EML4–ALK* fusion gene in non-small-cell lung cancer. *Nature* 2007; **448**: 561–6.
8 Hatanaka H, Takada S, Choi YL *et al.* Transforming activity of purinergic receptor P2Y, G-protein coupled, 2 revealed by retroviral expression screening. *Biochem Biophys Res Commun* 2007; **356**: 723–6.
9 Choi YL, Kaneda R, Wada T *et al.* Identification of a constitutively active mutant of JAK3 by retroviral expression screening. *Leuk Res* 2007; **31**: 203–9.
10 Brown AJ, Goldsworthy SM, Barnes AA *et al.* The Orphan G protein-coupled receptors GPR41 and GPR43 are activated by propionate and other short chain carboxylic acids. *J Biol Chem* 2003; **278**: 11312–9.
11 Fujiwara S, Yamashita Y, Choi YL *et al.* Transforming activity of purinergic receptor P2Y, G protein coupled, 8 revealed by retroviral expression screening. *Leuk Lymphoma* 2007; **48**: 978–86.
12 Pear WS, Nolan GP, Scott ML, Baltimore D. Production of high-titer helper-free retroviruses by transient transfection. *Proc Natl Acad Sci USA* 1993; **90**: 8392–6.
13 Schaeren-Wiemers N, Gerfin-Moser A. A single protocol to detect transcripts of various types and expression levels in neural tissue and cultured cells: in

doi: 10.1111/j.1349-7006.2009.01348.x

situ hybridization using digoxigenin-labelled cRNA probes. *Histochemistry* 1993; **100**: 431–40.
14 Hong YH, Nishimura Y, Hishikawa D *et al.* Acetate and propionate short chain fatty acids stimulate adipogenesis via GPCR43. *Endocrinology* 2005; **146**: 5092–9.
15 Nilsson NE, Kotarsky K, Owman C, Olde B. Identification of a free fatty acid receptor, FFA2R, expressed on leukocytes and activated by short-chain fatty acids. *Biochem Biophys Res Commun* 2003; **303**: 1047–52.
16 Dass NB, John AK, Bassil AK *et al.* The relationship between the effects of short-chain fatty acids on intestinal motility in vitro and GPR43 receptor activation. *Neurogastroenterol Motil* 2007; **19**: 66–74.
17 Yonezawa T, Kobayashi Y, Obara Y. Short-chain fatty acids induce acute phosphorylation of the p38 mitogen-activated protein kinase/heat shock protein 27 pathway via GPR43 in the MCF-7 human breast cancer cell line. *Cell Signal* 2007; **19**: 185–93.
18 Karaki S, Mitsui R, Hayashi H *et al.* Short-chain fatty acid receptor, GPR43, is expressed by enteroendocrine cells and mucosal mast cells in rat intestine. *Cell Tissue Res* 2006; **324**: 353–60.
19 Karaki SI, Tazoe H, Hayashi H *et al.* Expression of the short-chain fatty acid receptor, GPR43, in the human colon. *J Mol Histol* 2008; **39**: 135–42.
20 Bergman EN. Energy contributions of volatile fatty acids from the gastrointestinal tract in various species. *Physiol Rev* 1990; **70**: 567–90.
21 Le Poul E, Loison C, Struyf S *et al.* Functional characterization of human receptors for short chain fatty acids and their role in polymorphonuclear cell activation. *J Biol Chem* 2003; **278**: 25481–9.
22 Cummings JH, Pomare EW, Branch WJ, Naylor CP, Macfarlane GT. Short chain fatty acids in human large intestine, portal, hepatic and venous blood. *Gut* 1987; **28**: 1221–7.
23 Topping DL, Clifton PM. Short-chain fatty acids and human colonic function: roles of resistant starch and nonstarch polysaccharides. *Physiol Rev* 2001; **81**: 1031–64.
24 Key TJ, Allen NE, Spencer EA, Travis RC. The effect of diet on risk of cancer. *Lancet* 2002; **360**: 861–8.
25 Reif S, Klein I, Lubin F, Farbstein M, Hallak A, Gilat T. Pre-illness dietary factors in inflammatory bowel disease. *Gut* 1997; **40**: 754–60.

Supporting Information

Additional Supporting Information may be found in the online version of this article:

Table S1. Gallbladder cancer cDNA isolated from 3T3 transformants.

Please note: Wiley-Blackwell are not responsible for the content or functionality of any supporting materials supplied by the authors. Any queries (other than missing material) should be directed to the corresponding author for the article.

Cancer Science
The official journal of the Japanese Cancer Association

Identification of the transforming activity of Indian hedgehog by retroviral expression screening

Hisashi Hatanaka,[1,2] Shuji Takada,[1] Mamiko Tsukui,[2] Young Lim Choi,[1,4] Kentaro Kurashina,[3] Manabu Soda,[1] Yoshihiro Yamashita,[1] Hidenori Haruta,[1] Toru Hamada,[1] Kiichi Tamada,[2] Yoshinori Hosoya,[3] Naohiro Sata,[3] Hideo Nagai,[3] Yoshikazu Yasuda,[3] Kentaro Sugano[2] and Hiroyuki Mano[1,4,5,6]

Divisions of [1]Functional Genomics and [2]Gastroenterology, [3]Department of Surgery, Jichi Medical University, Tochigi; [4]Department of Medical Genomics, Graduate School of Medicine, The University of Tokyo, Tokyo; [5]CREST, Japan Science and Technology Agency, Saitama, Japan

(Received May 10, 2009/Revised August 29, 2009/Accepted September 2, 2009/Online publication September 30, 2009)

To identify novel cancer-promoting genes in biliary tract cancer (BTC), we constructed a retroviral cDNA expression library from a clinical specimen of BTC with anomalous pancreaticobiliary duct junction (APBDJ), and used the library for a focus formation assay with 3T3 fibroblasts. One of the cDNAs rescued from transformed foci was found to encode Indian hedgehog homolog (IHH). The oncogenic potential of IHH was confirmed both *in vitro* with the focus formation assay and *in vivo* with a tumorigenicity assay in nude mice. The isolated *IHH* cDNA had no sequence alterations, suggesting that upregulation of IHH expression may contribute to malignant transformation. Quantitation of *IHH* mRNA among clinical specimens has revealed that the expression level of *IHH* in BTC with APBDJ is higher than that in BTC without APBDJ and than in non-cancerous biliary tissues. Our data thus implicate a direct role of IHH in the carcinogenesis of BTC with APBDJ. (*Cancer Sci* 2010; 101: 60–64)

Biliary tract cancer (BTC) is a highly fatal malignancy in humans, and is prevalent in South American and Asian countries; approximately sixteen thousand people die of BTC every year in Japan.[1] Unfortunately, many BTC cases are diagnosed at advanced clinical stages with a 5-year survival rate of ~10%.[2–4] Several risk factors for BTC have been identified to date, including cholelithiasis,[5] anomalous pancreaticobiliary duct junction (APBDJ),[6] and primary sclerosing cholangitis.[7] Genetic alternations in *KRAS* or *TP53* and/or overexpression of *ERBB2* have been shown to contribute to the development of certain types of BTC. However, many cases with BTC do not harbor any such genetic changes, and other transforming events further await discovery.

The focus formation assay with 3T3 or RAT1 fibroblasts has been extensively used to screen for transforming genes in various carcinomas.[8] In such screening, genomic DNA is isolated from cancer specimens, and used to transfect 3T3 fibroblasts to obtain transformed cell foci. As expression of transfected genes in 3T3 cells in this assay is regulated by their own promoter and enhancer fragments, oncogenes with tissue-specific expression (e.g. those with a blood cell-specific promoter) can not become transcriptionally active in 3T3 cells, and thus can no longer be captured in such a screening system.

To ensure the sufficient expression of oncogenes in 3T3 cells, their transcription should be directly regulated by an exogenous promoter fragment. We have therefore constructed a retroviral cDNA expression library from a surgically operated clinical specimen of BTC with APBDJ, which was subsequently used to infect 3T3 cells. In the preparation of the cDNA library, we further took advantage of the SMART PCR system (Clontech, Mountain View, CA, USA), which preferentially amplifies full-length cDNA. A focus formation assay with the library has resulted in the identification of a transforming Indian hedgehog homolog (*IHH*) cDNA.

Materials and Methods

Focus formation assay with a retroviral library. A recombinant retroviral library was constructed as described previously,[9–12] with minor modifications. In brief, total RNA was extracted from a BTC specimen with APBDJ isolated from a 67-year-old man, who gave informed consent. This study was approved by the ethics committee of Jichi Medical University. First-strand cDNA was synthesized from the RNA with the use of PowerScript reverse transcriptase, the SMART IIA oligonucleotide, and CDS primer IIA (all from Clontech). The resulting cDNA was then amplified by PCR with 5′-PCR primer IIA (Clontech) and PrimeSTAR HS DNA polymerase (Takara Bio, Shiga, Japan) for 18 cycles of 98°C for 10 s and 68°C for 6 min. The PCR products were ligated to a *Bst*XI adapter (Invitrogen, Carlsbad, CA, USA) and then incorporated into the pMXS retroviral plasmid (kindly provided by T. Kitamura of the Institute of Medical Science, University of Tokyo). A total of 5.8×10^5 colony forming units of independent plasmid clones was thus generated. Twenty clones were randomly isolated from the library, and examined for the incorporated cDNA. Sixteen (80%) out of the 20 clones contained cDNA inserts with an average length of 1.16 kbp. Recombinant retroviruses were produced by introduction of the plasmid library into the packaging cell line BOSC23 (American Type Culture Collection, Manassas, VA, USA) and were used to infect 3T3 cells in the presence of 4 μg/mL polybrene (Sigma, St Louis, MO, USA). The cells were cultured for 2 weeks, after which transformed foci were isolated, expanded, and subjected to extraction of genomic DNA. Insert cDNA was recovered from the genomic DNA by PCR with 5′-PCR primer IIA and PrimeSTAR HS DNA polymerase. Amplified products were then ligated to the plasmid pT7Blue-2 (Novagen, Madison, WI, USA) and subjected to nucleotide sequencing.

Tumorigenicity assay in nude mice. 3T3 cells (2×10^6) were infected with a retrovirus expressing IHH, resuspended in 500 μL PBS, and injected into each shoulder of a *nu/nu* Balb-c mouse (6 weeks old). Tumor formation was assessed after 2 weeks.

Anchorage-independent growth in soft agar. 3T3 cells (2×10^6) were infected with a retrovirus encoding IHH or v-Ras, resuspended in the culture medium supplemented with 0.4% agar (Sea Plaque GTG agarose; Cambrex, East Rutherford, NJ, USA), and seeded onto a base layer of complete medium supplemented with 0.5% agar. Cell growth was assessed after culture for 2–3 weeks.

Quantitative RT-PCR analysis. Portions of oligo(dT)-primed cDNA produced by reverse transcription were subjected to PCR with a QuantiTect SYBR Green PCR kit (Qiagen, Valencia, CA, USA) and an amplification protocol comprising incubation at 94°C for 15 s, 60°C for 30 s, and 72°C for 60 s. Incorporation

[6]To whom correspondence should be addressed. E-mail: hmano@jichi.ac.jp

doi: 10.1111/j.1349-7006.2009.01355.x

of the SYBR Green dye into PCR products was monitored in real time with an ABI PRISM 7900HT sequence detection system (Applied Biosystems, Foster City, CA, USA), thereby allowing determination of the threshold cycle (C_T) at which exponential amplification of PCR products begins. The C_T values for cDNA corresponding to the β-actin gene (*ACTB*) and *IHH* were used to calculate the abundance of the latter mRNA relative to that of the former. The oligonucleotide primers used for PCR were 5′-CCATCATGAAGTGTGACGTGG-3′ and 5′-GTCCGCCTAGAAGCATTTGCG-3′ for *ACTB* and 5′-CCTCTCTCCTAGAGACCTTG-3′ and 5′-CTGGCTCCCAGGGAATTTAG-3′ for *IHH*.

Immunohistochemistry. Human tissues were fixed in 4% formaldehyde in PBS overnight at room temperature, embedded in paraffin, and sectioned at a thickness of 3 μm. Sections were mounted on glass slides, deparaffinized in three changes of xylene for 4 min each, and rehydrated in distilled water through a series of graded alcohols. For histological evaluation, sections were stained with hematoxylin–eosin. For immunohistochemical experiments, antigenicity was enhanced by boiling the sections in 10 mM citrate buffer (pH 6.0) in a microwave oven for 15 min, and the endogenous peroxidase activity was blocked by incubation in methanol containing 0.3% H_2O_2 for 30 min. After two washes with PBS containing 1% Triton X-100, the sections were preincubated with the blocking buffer (#X0909; Dako, Glostrup, Denmark) in a humidified chamber for 20 min at room temperature, and then incubated overnight at 4°C with anti-IHH antibody (sc-1196; Santa Cruz Biochemistry, Santa Cruz, CA, USA) diluted in PBS. Next, the sections were washed in PBS and incubated with horseradish peroxidase-labeled polymers conjugated to secondary antibodies for primary rabbit antigoat immunoglobulin (Dako, #P0449) without dilution at 37°C for 30 min. Color development was carried out by incubating the sections with 3,3-diaminobenzidine tetrahydrochloride (Wako Pure Chemical Industries, Osaka, Japan) as the chromogenic substrate. Finally, the sections were lightly counterstained with hematoxylin, mounted, and viewed under a light microscope. For the negative control, the immunostaining processes were carried out by replacing the primary antibody with PBS.

Results

Screening with the focus formation assay. From the mRNA of a BTC specimen with APBDJ, full-length cDNA was selectively amplified and ligated to a retroviral vector pMXS. From such library plasmids, we generated a recombinant ecotropic retrovirus that was subsequently used to infect mouse 3T3 fibroblasts. Infection experiments were repeated for a total of four times. After 3 weeks of culture, 75 transformed foci were observed. No foci could be found among the cells infected with an empty virus, while numerous foci were easily identified in the cells infected with a virus expressing v-Ras oncoprotein (data not shown).

Table 1. Bile duct cancer cDNA isolated from 3T3 transformants

Clone ID #	Gene symbol	GenBank no.	Presence of full ORF
1	*FAM83H*	NM_198488	No
2	*GATAD1*	NM_021167	Yes
3	*RRAS2*	NM_012250	No
4	*FASTK*	NM_006712	Yes
5	*VAT1*	NM_006373	Yes
6	*ARPC2*	NM_005731	No
7	*IHH*	NM_002181	Yes
8	*SENP6*	NM_015571	Yes
9	*DOT1L*	NM_032482	ND
10	*LTBR*	NM_002342	ND
11	*KRAS*	NM_004985	Yes
12	*TMEM54*	NM_033504	Yes
13	*RNASET2*	NM_003730	Yes
14	*RPS4X*	NM_001007	Yes
15	*TETRAN*	NM_001120	Yes
16	*DFNB31*	NM_015404	No
17	*CLDN3*	NM_001306	No
18	*GJB2*	NM_004004	Yes
19	*PSMA7*	NM_002792	Yes
20	*PRPSAP1*	NM_002766	Yes
21	*LRRC59*	NM_018509	Yes
22	*LRP5*	NM_002335	ND
23	*NCOR2*	NM_006312	No
24	*KLF16*	NM_031918	No
25	*ARHGAP4*	NM_001666	ND
26	*KIAA0284*	NM_015005	No
27	*DNAJC4*	NM_005528	ND
28	*NOTCH2NL*	NM_203458	No
29	*BCKDHB*	NM_000056	Yes

ND, not determined; ORF, open reading frame.

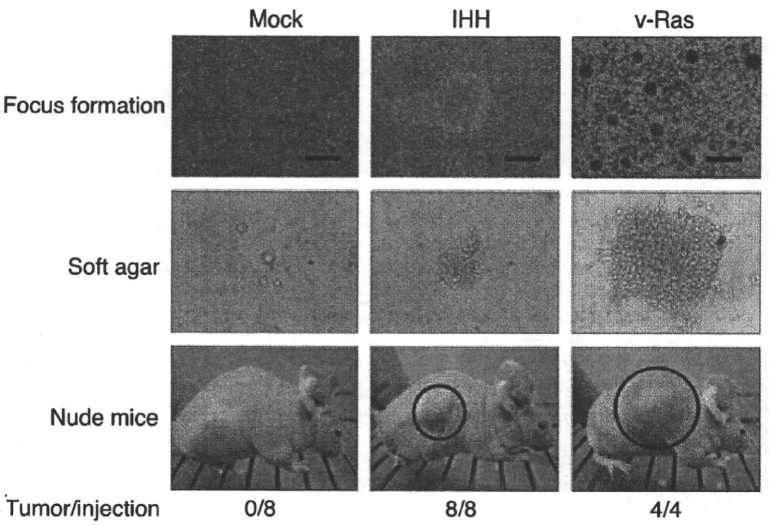

Fig. 1. Transforming activity of Indian hedgehog homolog (IHH). Mouse 3T3 cells were infected with viruses encoding IHH or v-Ras or with the empty virus (Mock), and were then cultured for 5 days for the analysis of focus formation (top panels; scale bars = 1 mm). The same batches of 3T3 cells were also assayed for anchorage-independent growth in soft agar over 17 days (middle panels) and for tumorigenicity in nude mice over 3 weeks (bottom panels). Tumors formed in the shoulders of mice injected subcutaneously with 1×10^5 cells are indicated by red circles. The frequency of tumor formation (tumors/injection) is also indicated.

Each focus was isolated, expanded independently, and used to prepare genomic DNA. We then tried to recover retroviral inserts from such genomic DNA by PCR amplification with the primer used originally to amplify the cDNA in the construction of the library. In most cases, one to three DNA fragments were recovered from each genome, implying multiple retroviral infection of some 3T3 cells.

We finally obtained a total of 44 cDNA fragments by PCR, each of which was ligated into a cloning vector, and subjected to nucleotide sequencing from both ends. Screening of the 44 cDNA sequences against the public nucleotide sequence databases revealed that the 44 fragments correspond to 29 independent genes (Table 1).

Identification of IHH. To confirm the transforming potential of the isolated cDNA, each cDNA clone was ligated to pMXS, and corresponding retrovirus was used to re-infect 3T3 cells. Focus formation assays were conducted for 13 independent genes, discovering a reproducible transforming activity for clone ID #7 corresponding to *IHH* (GenBank accession number, NM_002181) (Fig. 1, top panel). Again, infection with a virus for v-Ras induced many transformed foci, while an empty virus failed to do so. The entire coding region of our ID #7 cDNA was sequenced, revealing no point mutations or deletions compared to the published *IHH* cDNA sequence. Although activation of Hedgehog (Hh) pathways has been revealed among a wide range of digestive tract cancers,[13] oncogenic activity of *IHH* has not been reported to date. We supposed from our data that overexpression of *IHH* may contribute directly to malignant transformation.

Confirmation of the transforming activity of IHH. To confirm the oncogenic activity of IHH, we examined its effect on the anchorage-independent growth of 3T3 cells in soft agar. Whereas cells infected with an empty virus did not grow in the agar, those infected with a virus expressing IHH formed multiple foci in repeated experiments (Fig. 1, middle panel). In addition, 3T3 cells expressing v-Ras readily grew in the agar.

The transforming activity of IHH was also tested by the tumor formation assay with athymic nude mice. 3T3 cells infected with the empty virus or retrovirus expressing IHH or v-Ras were inoculated subcutaneously into nude mice. As shown in the bottom panel of Fig. 1, tumor formation was readily observed for the cells expressing IHH or v-Ras. These results clearly revealed an unexpected, direct transforming potential of IHH in fibroblasts.

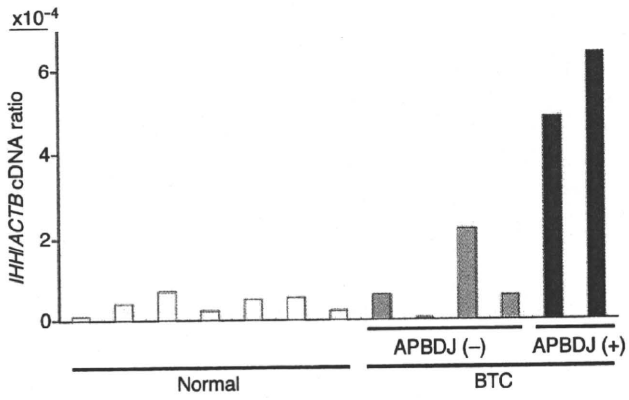

Fig. 2. Expression of Indian hedgehog homolog (*IHH*) in biliary tract. Oligo(dT)-primed cDNA was synthesized from clinical specimens of biliary tract cancer (BTC) with (+) or without (–) anomalous pancreaticobiliary duct junction (APBDJ), or from normal gallbladder (Normal), and were subjected to quantitative PCR analysis for cDNA of *IHH* and β-actin (*ACTB*). The relative expression level of the former to the latter is represented.

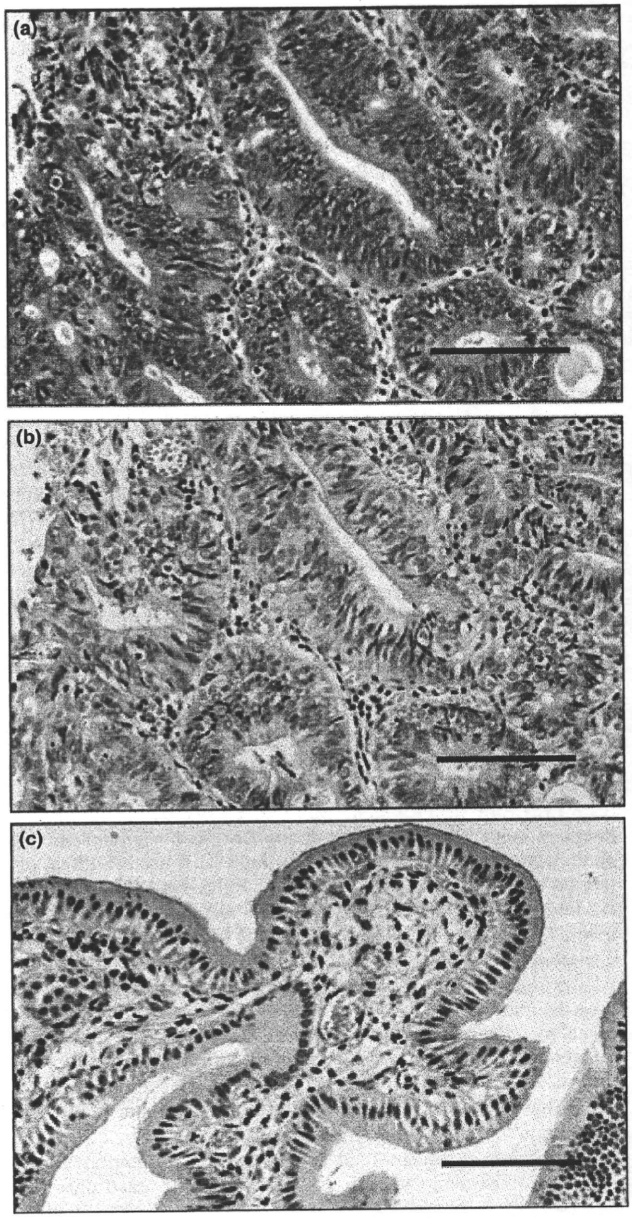

Fig. 3. Immunohistochemical detection of Indian hedgehog homolog (IHH). Expression of IHH is elevated in (a) biliary tract cancer with anomalous pancreaticobiliary duct junction, but such reactivity was absent in the control experiment for (b) the same specimen or (c) anti-IHH staining in normal gallbladder. Scale bars = 100 μm.

Overexpression of *IHH* mRNA. Given the transforming potential of wild-type IHH (when it is abundantly expressed), we tried to examine if *IHH* is overexpressed in BTC specimens. Real-time RT-PCR analysis for the quantitation of *IHH* cDNA among normal gall bladder ($n = 7$) and BTC specimens ($n = 6$) (Supporting Information Table S1) revealed that *IHH* is indeed overexpressed in the latter specimens, albeit with marginal statistical significance ($P = 0.06$) by a two-tailed t-test (Fig. 2). It should be noted, however, that BTC cases with APBDJ ($n = 2$) had significantly abundant expression of *IHH* compared to BTC

doi: 10.1111/j.1349-7006.2009.01355.x

without APBDJ ($P = 0.005$) or to normal gall bladder ($P = 2.4 \times 10^{-6}$). Therefore, it is likely that some types of BTC overexpress IHH.

Protein expression of IHH. To confirm the elevated expression of IHH in BTC, we examined its protein level by an immunohistochemical approach. In accordance with the RT-PCR experiments, IHH protein was abundantly detected only in the cytoplasm of cancerous duct but not in stromal cells for BTC with APBDJ (Fig. 3). We failed to observe such staining in normal gallbladder, suggesting that IHH protein was markedly induced in BTC with APBDJ compared to normal gallbladder.

Discussion

In the present study, we have constructed a retroviral cDNA expression library for a BTC specimen with APBDJ, and unexpectedly revealed the transforming potential of IHH through a focus formation assay with the mouse fibroblast cell line 3T3. As there were no sequence alterations in our isolated *IHH* cDNA, the high expression of IHH is likely to exert its oncogenic activity. Consistent with this notion, expression of *IHH* was indeed activated in BTC with APBDJ.

In our transformation assays for IHH (i.e. focus formation assay, soft agar-growth assay, and nude mouse-tumorigenicity assay) we directly used a highly polyclonal, mass culture of 3T3 cells infected with a retrovirus expressing IHH, without any selection (such as positive selection for neomycin resistance-cells). Repeated confirmation of the transforming potential for IHH in such assays (and not for an empty virus) strongly argues against a hypothesis that an artificial expression of mouse genes adjacent to the retroviral integration sites was responsible for the 3T3 transformation in these experiments.

The Hh signaling pathway was originally described in the development of *Drosophila melanogaster* as a segment polarity gene required for embryonic patterning.[14] There are three vertebrate homologues of Hh: Ihh, Sonic hedgehog (Shh), and Desert hedgehog (Dhh) with similar biological properties among them. Hh signaling is known to play a pivotal role in cell fate decisions,[15] tissue repair,[16] and stem cell self renewal.[17,18] Aberration in such signaling may contribute to sustained cell growth and cancer. Indeed, Hahn *et al.* and Johnson *et al.* revealed that mutations within *PTCH1* (a binding partner of hedgehog) cause a cancer-promoting condition, Gorlin syndrome.[19,20] Further, frequent mutations in Hh signaling components have also been identified among sporadic basal cell carcinoma[21] and medulloblastoma.[22]

In addition, transcriptional activation of Hh components has been demonstrated among a wide range of gastrointestinal tumors, which results from endogenous overexpression of Hh proteins such as IHH and SHH.[13] Despite the lack of gene mutations for the Hh components in these tumors, cyclopamine, a specific inhibitor for SMO, suppresses the growth of tumors positive for elevated Hh signaling, supporting the idea that overexpression of the Hh family of proteins may have a mitogenic function.

Our current data proves for the first time the direct transforming potential of IHH, at least in fibroblasts. Furthermore, apparent overexpression of *IHH* in BTC with APBDJ indicates an important role of IHH especially in this subtype of BTC. In addition to the presence or absence of APBDJ, we also examined the clinicopathological features of the BTC specimens used in our study. As shown in Supporting Information Table S1, none of the TNM stage, clinical stage, KRAS mutation, or Ki-67 index were related to the overexpression of *IHH*. However, because the current cohort size is still small, a larger cohort study is mandatory to examine the clinical features of BTC with high *IHH*.

Although Yang *et al.* reported that treatment with a SMO inhibitor leads to downregulation of *CCND1* and upregulation of *CDKN1A* in a cell line of pancreatic carcinoma,[23] we did not observe such a relationship between *CCND1/CDKN1A* and *IHH* expression (data not shown). However, overexpression of *CCND1* may be more prevalent among BTC than that of *IHH*,[24] suggesting the presence of an IHH-independent regulatory network for *CCND1* in BTC.

APBDJ causes pancreatic fluid regurgitation into the biliary duct, and is found frequently among BTC cases.[25] Because pancreatic fluid is rich in various proteases, frequent regurgitation of such fluid into the biliary tract is likely to cause sustained inflammation in the tract. Because inflammation and tissue repair cause transcriptional activation of the Hh family of soluble factors,[16] it may not be surprising to find an elevated level of *IHH* mRNA in the biliary tract with APBDJ. Given the transforming function of abundant IHH, such overexpression may lead to increased cell cycle of biliary tract cells, and eventually to the generation of BTC. Because a number of chemical inhibitors are under development for the Hh pathways,[26] BTC with APBDJ would be an intriguing candidate for such drugs. Further, it is also tempting to examine the Hh ligand levels among human cancers associated with chronic inflammation or regeneration.

Acknowledgments

This work was supported in part by grants for Research on Human Genome and Tissue Engineering and for Third-Term Comprehensive Control Research for Cancer from the Ministry of Health, Labor, and Welfare of Japan, as well as by a grant for Scientific Research on Priority Areas "Applied Genomics" from the Ministry of Education, Culture, Sports, Science, and Technology of Japan.

Abbreviations

CCND1	cyclin D1
CDKN1A	cyclin-dependent kinase inhibitor 1A
ERBB2	v-erb-b2 avian erythroblastic leukemia viral oncogene homolog 2
KRAS	v-ki-ras2 Kirsten rat sarcoma viral oncogene homolog
PTCH1	Patched, Drosophila, homolog of, 1
TP53	tumor protein p53

References

1 National Cancer Center. *Cancer statistics in Japan 2007 (Website on the internet)*. Tokyo, Japan: National Cancer Center, 2008. [Cited 16 November 2007.] Available from URL: http://www.ganjoho.jp/public/statistics/backnumber/2007_en.html.
2 Carriaga MT, Henson DE. Liver, gallbladder, extrahepatic bile ducts, and pancreas. *Cancer* 1995; **75**: 171–90.
3 Cubertafond P, Gainant A, Cucchiaro G. Surgical treatment of 724 carcinomas of the gallbladder. Results of the French Surgical Association Survey. *Ann Surg* 1994; **219**: 275–80.
4 Shaib Y, El-Serag HB. The epidemiology of cholangiocarcinoma. *Semin Liver Dis* 2004; **24**: 115–25.
5 Zatonski WA, Lowenfels AB, Boyle P *et al.* Epidemiologic aspects of gallbladder cancer: a case-control study of the SEARCH Program of the International Agency for Research on Cancer. *J Natl Cancer Inst* 1997; **89**: 1132–8.

6 Hasumi A, Matsui H, Sugioka A *et al.* Precancerous conditions of biliary tract cancer in patients with pancreaticobiliary maljunction: reappraisal of nationwide survey in Japan. *J Hepatobiliary Pancreat Surg* 2000; **7**: 551–5.
7 Rosen CB, Nagorney DM, Wiesner RH, Coffey RJ Jr, LaRusso NF. Cholangiocarcinoma complicating primary sclerosing cholangitis. *Ann Surg* 1991; **213**: 21–5.
8 Aaronson SA. Growth factors and cancer. *Science* 1991; **254**: 1146–53.
9 Soda M, Choi YL, Enomoto M *et al.* Identification of the transforming *EML4–ALK* fusion gene in non-small-cell lung cancer. *Nature* 2007; **448**: 561–6.
10 Hatanaka H, Takada S, Choi YL *et al.* Transforming activity of purinergic receptor P2Y, G-protein coupled, 2 revealed by retroviral expression screening. *Biochem Biophys Res Commun* 2007; **356**: 723–6.
11 Fujiwara S, Yamashita Y, Choi YL *et al.* Transforming activity of purinergic receptor P2Y, G protein coupled, 8 revealed by retroviral expression screening. *Leuk Lymphoma* 2007; **48**: 978–86.
12 Choi YL, Kaneda R, Wada T *et al.* Identification of a constitutively active mutant of JAK3 by retroviral expression screening. *Leuk Res* 2007; **31**: 203–9.
13 Berman DM, Karhadkar SS, Maitra A *et al.* Widespread requirement for Hedgehog ligand stimulation in growth of digestive tract tumours. *Nature* 2003; **425**: 846–51.
14 Nusslein-Volhard C, Wieschaus E. Mutations affecting segment number and polarity in Drosophila. *Nature* 1980; **287**: 795–801.
15 Ingham PW, McMahon AP. Hedgehog signaling in animal development: paradigms and principles. *Genes Dev* 2001; **15**: 3059–87.
16 Beachy PA, Karhadkar SS, Berman DM. Tissue repair and stem cell renewal in carcinogenesis. *Nature* 2004; **432**: 324–31.
17 Liu S, Dontu G, Wicha MS. Mammary stem cells, self-renewal pathways, and carcinogenesis. *Breast Cancer Res* 2005; **7**: 86–95.
18 Liu S, Dontu G, Mantle ID *et al.* Hedgehog signaling and Bmi-1 regulate self-renewal of normal and malignant human mammary stem cells. *Cancer Res* 2006; **66**: 6063–71.
19 Hahn H, Wicking C, Zaphiropoulous PG *et al.* Mutations of the human homolog of Drosophila patched in the nevoid basal cell carcinoma syndrome. *Cell* 1996; **85**: 841–51.
20 Johnson RL, Rothman AL, Xie J *et al.* Human homolog of patched, a candidate gene for the basal cell nevus syndrome. *Science* 1996; **272**: 1668–71.
21 Reifenberger J, Wolter M, Weber RG *et al.* Missense mutations in SMOH in sporadic basal cell carcinomas of the skin and primitive neuroectodermal tumors of the central nervous system. *Cancer Res* 1998; **58**: 1798–803.
22 Taylor MD, Liu L, Raffel C *et al.* Mutations in SUFU predispose to medulloblastoma. *Nat Genet* 2002; **31**: 306–10.
23 Yang Y, Tian X, Xie X, Zhuang Y, Wu W, Wang W. Expression and regulation of hedgehog signaling pathway in pancreatic cancer. *Langenbecks Arch Surg* 2009; doi. 10.1007/s00423-009-0493-9.
24 Hui AM, Li X, Shi YZ, Takayama T, Torzilli G, Makuuchi M. Cyclin D1 overexpression is a critical event in gallbladder carcinogenesis and independently predicts decreased survival for patients with gallbladder carcinoma. *Clin Cancer Res* 2000; **6**: 4272–7.
25 Kimura K, Ohto M, Saisho H *et al.* Association of gallbladder carcinoma and anomalous pancreaticobiliary ductal union. *Gastroenterology* 1985; **89**: 1258–65.
26 Rubin LL, de Sauvage FJ. Targeting the Hedgehog pathway in cancer. *Nat Rev Drug Discov* 2006; **5**: 1026–33.

Supporting Information

Additional Supporting Information may be found in the online version of this article:

Table S1. Clinical characteristics of the patients with biliary tract cancer (BTC).

Please note: Wiley-Blackwell are not responsible for the content or functionality of any supporting materials supplied by the authors. Any queries (other than missing material) should be directed to the corresponding author for the article.

doi: 10.1111/j.1349-7006.2009.01355.x

INTERNAL MEDICINE

□ ORIGINAL ARTICLE □

Clinical Features of Lymphangioleiomyomatosis Complicated by Renal Angiomyolipomas

Yoshiko Mizushina, Masashi Bando, Tatsuya Hosono, Naoko Mato, Takakiyo Nakaya, Yoshikazu Ishii, Hideaki Yamasawa and Yukihiko Sugiyama

Abstract

Objective Renal angiomyolipomas (R-AMLs) are major complications of lymphangioleiomyomatosis (LAM). The objective of this study was to better understand the influence of R-AMLs in patients with LAM on the prognosis and other clinical factors related to respiration, and to investigate the management of R-AMLs in patients with LAM.

Patients and Methods We retrospectively investigated the clinical features of 7 patients with LAM [4 were TSC (Tuberous sclerosis complex)-LAM and 3 were S (sporadic)-LAM] complicated by R-AMLs admitted to our hospital from 1997 to 2008.

Results All patients were females and the mean age at diagnosis of LAM was 40.7 years (31.7 years for TSC-LAM and 52.7 years for S-LAM). Although 5 patients had symptoms related to R-AMLs, only 1 patient experienced symptoms related to R-AMLs at the time of diagnosis. Five patients had bilateral and 2 patients had unilateral R-AMLs. R-AMLs ruptured in 4 cases (3 patients were TSC-LAM) including 2 patients in whom they ruptured bilaterally, and who underwent bilateral nephrectomy. In 1 case, unilateral R-AMLs grew larger and appeared on the other side during the follow-up period.

Conclusion Although only rare cases of LAM show symptoms related to R-AMLs initially, R-AMLs are a notable complication. To avoid nephrectomy, R-AMLs should be diagnosed when they are small and should be followed up carefully by periodic echograms or CT scans.

Key words: lymphangioleiomyomatosis, renal angiomyolipoma, tuberous sclerosis complex, total nephrectomy

(Intern Med 50: 285-289, 2011)
(DOI: 10.2169/internalmedicine.50.3558)

Introduction

Lymphangioleiomyomatosis (LAM) is a rare disease that occurs predominantly in females and is characterized by the proliferation of smooth muscle cells and cyst formation. LAM occurs in 30% of patients with tuberous sclerosis complex (TSC), but patients with LAM complicated by TSC (TSC-LAM) constitute only approximately 15% of all LAM cases. The remaining cases are sporadic LAM (S-LAM). LAM patients have renal angiomyolipomas (R-AMLs) in about 93% of TSC-LAM and about 30-50% of S-LAM cases (1).

In order to better understand the influence of R-AMLs in patients with LAM on the prognosis and other clinical factors related to respiration, and to investigate the management of R-AMLs in patients with LAM, we retrospectively investigated 7 cases of LAM complicated by R-AMLs who were admitted to our hospital from 1997 to 2008.

Patients and Methods

Thirteen patients with LAM were admitted to our hospital from 1977 to 2008. We investigated the clinical features of 7 patients with LAM (4 were TSC-LAM and 3 were S-LAM) complicated by R-AMLs. Retrospective chart reviews were performed on each case. The size of the R-AMLs were measured from echograms or computed tomography (CT)

Division of Pulmonary Medicine, Department of Medicine, Jichi Medical University, Japan
Received for publication February 18, 2010; Accepted for publication October 11, 2010
Correspondence to Dr. Yoshiko Mizushina, mizushina@jichi.ac.jp

Table 1. Clinical Characteristics of 13 LAM Cases

Case No.	Age of diagnosis as LAM*1	Age of initial symtoms	R-AMLs *2	TSC *3	Initial symtoms	Symptoms of R-AMLs	Pneumothorax	Duration until induction of HOT*4 from initial symptoms[years]	Decline of VC*5/year[ml]	Decline of $FEV_{1.0}$*6/year[ml]	Therapy	Follow up period from diagnosis	Respiratory failure
1	32	27	+	-	Chest pain	Abdominal pain	+	-			progesteron	26 years	-
2	58	50	+	-	Dyspnea on exertion	Abdominal pain	+	11	12.86	51.43		Induction of IPPV for respiratory failure after 9 years	+
3	42	41	+	-	Dyspnea on exertion	-	-	13	1.54	52.31	progesteron	Progression of respiratory failure Transfer to another hospital after 16 years	+
4	34	32	+	+	Dyspnea on exertion	Abdominal pain and lumbago	+	3	136.67	79.17	progesteron	Progression of respiratory failure 14 years	+
5	29	29	+	+	Cough and fever	Appetite loss and nausea	-	-	-5.00	-21.67		Induction of hemodialysis 15 years	-
6	58	30	+	-	Pneumothorax	-	+	2				Dead of respiratory failure after 2 years Diagnosed by autopsy	+
7	32	31	+	+	Abdominal distention	Abdominal distention	+	-				2 years Renal transplantation was performed	-
8	42	39	-	-	Hemosputum		+	-	25.00	24.29		Progression of respiratory failure Dead of breast cancer after 17 years	+
9	46	40	-	-	Dyspnea on exertion		-	-				Dead of respiratory failure after 2 years Diagnosed by autopsy	+
10	38	37	-	-	Back pain		+	-	41.88	42.50		17 years	-
11	33	32	-	-	Cough and sputum		-	5	58.89	26.67	Progesteron +ovariectomy	Induction of IPPV for respiratory failure after 14 years	+
12	29	29	-	-	Cough and fever		-	-			progesteron	Drainage of chylothorax Transfer to another hospital after a year	-
13	29	27	-	-	Cough and lumbago		-	2	477.50	137.50	Progesteron LH-RH analog, Lung transplantation	Lung transplantation was performed after 3 years 3 years after transplantation	+

*1 LAM; Lymphangioleiomyomatosis, *2 R-AML; renal angiomyolipoma, *3 TSC; Tuberous sclerosis complex
*4 HOT; Home oxygen therapy, *5 VC; Vital capacity, *6 $FEV_{1.0}$; Forced expiratory volume in 1 second,

scans.

We diagnosed LAM using the diagnostic criteria established by the Respiratory Failure Research Group of the Japanese Ministry of Health, Labour and Welfare in 2005 (2).

We diagnosed R-AMLs based on echograms or CT scans. The appearance of R-AMLs on echogram is a strongly hyper-reflective lesion with acoustic shadowing. This appearance is a result of the multiple tissue interfaces between fatty and non-fatty components of the mass. The appearance of R-AMLs on unenhanced CT scan is a predominantly fatty inhomogeneous mass with varying amounts of tissue density interspersed within it. Minimal fat AMLs which contain only microscopically detectable fat account for 4.5% of R-AMLs. Although it is difficult to diagnose minimal fat AMLs by their appearance on echogram or CT scan, homogeneous enhancement and a prolonged enhancement pattern on CT scan are the most accurate predictors (3).

A statistical software package (Dr.SPSS II, for Windows; SPSS Inc.) was used for the analysis. Results are presented as the mean±standard error of the mean (SEM). The differences between the two groups were compared using Student's unpaired t-test. Fisher's exact test was calculated to assess relationships between the two parameters. A value of $p<0.05$ was considered statistically significant.

Case 7 was previously reported in 2008 in *Urology* (4).

Results

All of the patients were females and the mean age at diagnosis of LAM was 40.7 years. Seven cases were complicated by R-AMLs (Table 1).

All 4 patients (100%) with TSC-LAM had R-AMLs. Three of 9 patients (33%) with S-LAM had R-AMLs. The mean ages of patients at diagnosis of LAM with R-AMLs were 31.7 years for TSC-LAM patients and 52.7 years for S-LAM patients (Table 1). There were no significant differences between the groups with and without R-AMLs in the rates of pneumothorax ($p=0.21$) or respiratory failure ($p=0.63$).

Five patients had bilateral and 2 patients had unilateral R-AMLs. R-AMLs ruptured in 4 cases (3 patients were TSC-LAM), including 2 patients in whom they ruptured bilaterally. Renal artery embolization had been performed in 1 case, nephrectomy had been performed in 4 cases, and bilateral nephrectomy had been performed in the 2 cases with bilateral rupture (Table 2). Regarding changes in R-AMLs during the follow-up period, in 1 case (Case 1), unilateral R-AMLs grew larger (3 cm to 4 cm in 2 years) and appeared on the other side as well (Table 2). Four patients had hepatic angiomyolipomas and R-AMLs (3 were S-LAM and 1 was TSC-LAM) (Table 2).

Table 2. Clinical Course of 7 LAM Cases Complicated by Renal Angiomyolipomas

Case No.	R-AML*1	Size of R-AML	Rupture of R-AMLs	Intervention	Hepatic AML
1	Bilateral	Left 3→4cm; Right 0.5cm (2 years later)	-	Left nephrectomy	-
2	Left	Left 7 × 4cm	-		+
3	Bilateral	Left 0.5, 1and 3cm; Right 1cm	-		+
4	Bilateral	bilateral multiple 1-3cm nodules	Right	Arterial embolization	-
5	Bilateral	Left 8cm; Right 16cm	Bilateral	Bilateral nephrectomy	-
6	Left	Left 3cm(autopsy)	Left	Left nephrectomy	+
7	Bilateral	Left 36cm; Right 22cm	Bilateral	Bilateral nephrectomy	+

*1 R-AML; renal angiomyolipoma

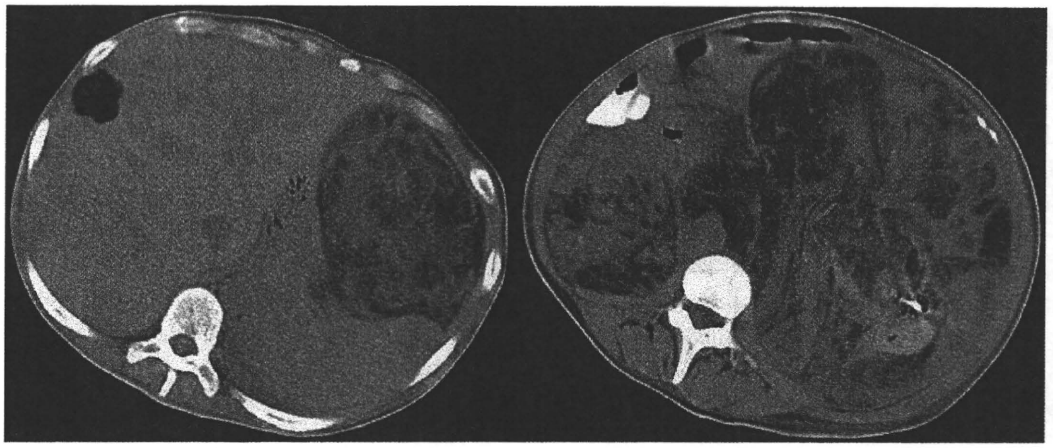

Figure 1. Giant bilateral renal angiomyolipomas in abdominal computed tomography (Case 7). Giant bilateral renal angiomyolipomas are shown in abdominal computed tomography. A hepatic angiomyolipoma is also shown. The patient experienced abdominal distention which was a symptom related to renal angiomyolipomas at the time of diagnosis.

Five patients visited our hospital due to respiratory symptoms (3 were dyspneic on exertion and 2 had symptoms related to pneumothorax) (Table 1). Although 5 patients had symptoms related to R-AMLs, only 1 patient (Case 7) experienced symptoms related to R-AMLs at the time of diagnosis (Fig. 1) (4).

We investigated the mean survival time, decline of vital capacity (VC) and decline of forced expiratory volume in 1 second ($FEV_{1.0}$). In the R-AMLs group, the mean survival time, decline of VC per year and decline of $FEV_{1.0}$ per year were 23.33±3.55 years, 36.5±67.1 mL and 40.3±43.2 mL, respectively. On the other hand, in the no R-AMLs group, the mean survival time, decline of VC per year and decline of $FEV_{1.0}$ per year were 14.20±2.50 years, 150.8±218.2 mL and 57.7±53.8 mL, respectively. There were no significant differences between the 2 groups in these 3 parameters (p= 0.66, p=0.09 and p=0.65, respectively).

Discussion

In the present study, 4 patients (100%) with TSC-LAM and 3 patients (33.3%) with S-LAM had R-AMLs. These results were compatible with those in previous reports showing that patients with LAM have R-AML in approximately 93% of TSC-LAM cases and 30-50% of S-LAM cases (1). In this study, although 5 patients showed symptoms related to R-AMLs, only 1 patient experienced symptoms related to R-AMLs at the time of diagnosis (4). The symptoms were relatively atypical at the time of diagnosis and might delay diagnosis. Therefore, this case is very important if we consider the history of LAM. The Respiratory Failure Research Group of the Japanese Ministry of Health, Labour and Welfare 2003-2004 reported on the epidemiology of LAM in Japan (5). In the report, 173 patients with LAM showed common presenting features of pneumothorax (43%), dyspnea on exertion (36%), abnormal shadow on chest radiograph (11%) and other respiratory symptoms (4%) such as haemoptysis, cough and chest pain. In contrast, only 6% of patients presented with abdominal manifestations attributable to LAM or R-AMLs (5). In Japan, although 12 cases with LAM complicated by R-AMLs have been reported previously (6-9), symptoms and diagnosis related to R-AMLs preceded the other symptoms in only 2 cases. The other 10 cases showed initial symptoms related to respiration. Pa-

tients with R-AMLs rarely show symptoms and gradually present lateroabdominal pain, hydronephrosis, hematuria and renal dysfunction during follow-up.

In this study, one patient initially had R-AMLs on the left side. These R-AMLs grew and a right R-AML appeared during follow-up. The clinical course of R-AMLs varies. Rakowski et al identified R-AMLs in 10-year-old children, and reported that they grow and increase during adolescence (10). It was reported that in one case, a 3 cm R-AML which was not detected by echogram at 21 years of age appeared when the individual was 23 years old, and that in another case, multiple R-AMLs that were not detected by echogram at 18 years of age appeared at 20 years of age (10). Therefore, especially in adolescents, we should look carefully for R-AMLs if they were not detected by echogram or CT scan at the initial diagnosis. When a patient is diagnosed as TSC, we should examine for R-AMLs by echogram by 5 years of age. Rakowski et al suggested that patients should be examined by echogram at least once a year if R-AMLs are found. If no R-AMLs are found, the patient should be examined for R-AMLs by echogram at least every two or three years (10).

In this study, 5 patients had bilateral R-AMLs, 2 patients had unilateral R-AMLs, and 2 patients underwent bilateral nephrectomy. All 4 cases of TSC-LAM had bilateral R-AMLs, and 3 of the 4 cases showed rupture of R-AMLs. In most cases with S-LAM, R-AMLs were unilateral, small and singular. On the other hand, in TSC-LAM cases, R-AMLs, including hepatic or splenic AMLs, were bilateral, larger, and multiple, and in addition, they bled easily (1). The risk of hemorrhage from R-AMLs is greater when they are larger and more hypervascular. In this study, the mean size of R-AMLs was 17.0±12.9 cm in the ruptured group and 3.1±2.6 cm in the non-ruptured group (p=0.04). Therefore, the choice of treatment should be evaluated for R-AMLs which are larger than 4 cm by echogram or CT scan, as suggested in a previous report (1). There was no significant difference in the risk of rupture of R-AMLs between the unilateral and bilateral groups (p=0.714). However, as mentioned above, in TSC-LAM cases, R-AMLs tend to be bilateral and bleed easily. Therefore caution should be exercised regarding rupture of R-AMLs in bilateral cases. Generally, we perform renal artery embolization, enucleation, ablation and partial nephrectomy. It was reported that a patient with R-AMLs larger than 10 cm was treated by nephron-sparing nephrectomy (8, 11). But it may be necessary to perform total nephrectomy in difficult cases (1). A delay in the diagnosis of R-AMLs sometimes results in bilateral nephrectomy and hemodialysis because a greater number of patients with LAM complicated by R-AMLs have bilateral R-AMLs. Therefore, we should diagnose R-AMLs without delay and avoid total nephrectomy as long as possible (12).

In recent years, LAM and AML were included in Perivascular epithelioid cell tumors (PEComa) which Bonetti et al proposed in 1992 (13). Alterations of the TSC genes have been demonstrated in a significant number of PEComas, and they seem to have an important role in the regulation of the Rheb/mTOR (mammalian target of rapamycin)/p70S6K pathway (14, 15). As mentioned above, in this study, all 4 patients with TSC-LAM and 3 of 10 patients with S-LAM had R-AMLs. PEComas may explain why TSC-LAM is more likely to complicate R-AMLs, although we did not investigate genetic alterations. There have been several clinical trials of agents targeting the mTOR pathway. The Cincinnati Angiomyolipoma Sirolimus Trial (CAST) showed that the volume of R-AMLs decreased by almost 50% after treatment for 1 year with the mTOR inhibitor (16). In addition, the Multicenter International LAM Efficacy of Sirolimus (MILES) Trial was initiated in 2006 (1, 17). But there are limitations for patients on hemodialysis for advanced R-AMLs receiving the mTOR inhibitor. These patients also face challenges undergoing lung transplantation, especially regarding perioperative management and using postoperative immunosuppressants, and have an uncertain prognosis.

In conclusion, although only rare cases of LAM show initial symptoms related to R-AMLs, R-AMLs are a notable complication. As advanced R-AMLs rupture easily, it is important to look carefully for R-AMLs while they are smaller than 4 cm by performing periodic echograms or CT scans. The choice of treatment should be evaluated for R-AMLs which are larger than 4 cm.

The authors state that they have no Conflict of Interest (COI).

References

1. McCormack FX. Lyphangioleiomyomatosis: a clinical update. Chest **133**: 507-516, 2008.
2. Hayashida M. Diagnostic criteria for lymphangioleiomyomatosis. Nihon Kokyuki Gakkai Zasshi (The Journal of the Japanese Respiratory Society) **46**: 425-427, 2008 (in Japanese).
3. Halpenny D, Snow A, McNeill G, Torreggiani WC. The radiological diagnosis and treatment of renal angiomyolipoma-current status. Clin Radiol **65**: 99-108, 2010.
4. Kobayashi M, Nakano K, Nukui A, Goto K, Morita T. Bilateral massive renal angiomyolipoma concurrent with oncocytoma in tuberous sclerosis complex associated with pulmonary lymphangioleiomyomatosis. Urology **72**: 948.e7-948.e9, 2008.
5. Hayashida M, Seyama K, Inoue Y, Fujimoto K, Kubo K. Respiratory Failure Research Group of the Japanese Ministry of Health, Labor, and Welfare. The epidemiology of lymphangioleiomyomatosis in Japan: a nationwide cross-sectional study of presenting features and prognostic factors. Respirology **12**: 523-530, 2007.
6. Kano N, Hayashi K, Itaya N, et al. A case of renal angiomyolipoma with pulmonary lymphangioleiomyomatosis. Hinyokigeka (Japanese Journal of Urological Surgery) **20**: 817-819, 2007 (in Japanese, Abstract in English).
7. Saito J, Kakuta Y, Yazawa K, Hosomi M, Sagawa S, Ito K. Renal angiomyolipoma in association with lymphangioleiomyomatosis. Rinsho Hinyokika (Japanese Journal of Clinical Urology) **60**: 843-845, 2006 (in Japanese, Abstract in Engligh).
8. Niimi A, Kume H, Kumano S, et al. Giant renal angiomyolipoma in a case with pulmonary lymphangiomyomatosis. Nippon Hinyokika Gakkai Zasshi (The Journal of the Japanese Respiratory Society) **98**: 713-717, 2007 (in Japanese, Abstract in

Engligh).

9. Miyake M, Tateishi U, Maeda T, et al. Pulmonary lymphangioleiomyomatosis in a male patient with tuberous sclerosis complex. Radiat Med **23**: 525-527, 2005.
10. Rakowski SK, Winterkorn EB, Paul E, Steele DJ, Halpern EF, Thiele EA. Renal manifestations of tuberous sclerosis complex: Incidence, prognosis, and predictive factors. Kidney Int **70**: 1777-1782, 2006.
11. Hsu TH, O'Hara J, Mehta A, Levitin A, Klein EA. Nephron-sparing nephrectomy for giant renal angiomyolipoma associated with lymphangioleiomyomatosis. Urology **59**: 138, 2002.
12. Bernstein SM, Newell JD Jr, Adamczyk D, Mortenson RL, King TE Jr, Lynch DA. How common are renal angiomyolipomas in patients with pulmonary lymphangiomyomatosis? Am J Respir Crit Care Med **152**: 2138-2143, 1996.
13. Bonetti F, Pea M, Martignoni G, Zamboni G. PEC and sugar. Am J Surg Pathol **16**: 307-308, 1992.
14. Pan CC, Chung MY, Ng KF, et al. Constant allelic alteration on chromosome 16p (TSC2 gene) in perivascular epithelioid cell tumour (PEComa): genetic evidence for the relationship of PEComa with angiomyolipoma. J Pathol **214**: 387-393, 2008.
15. Martignoni G, Pea M, Reghellin D, Zamboni G, Bonetti F. PEComas: the past, the present and the future. Virchows Arch **452**: 119-132, 2008.
16. Bissler JJ, McCormack FX, Young LR, et al. Sirolimus for angiomyolipoma in tuberous sclerosis complex or lymphangioleiomyomatosis. N Engl J Med **358**: 140-151, 2008.
17. Rare Diseases Clinical Research Network (RDCRN). Clinical Studies5702: Multicenter International Lymphangioleiomyomatosis Efficacy of Sirolimus Trial (MILES). http://rarediseasesnetwork.epi.usf.edu/rldc/takeaction/studies/miles-5702.htm

Am J Physiol Lung Cell Mol Physiol 298: L348–L360, 2010.
First published December 24, 2009; doi:10.1152/ajplung.00289.2009.

Therapeutic effect of lecithinized superoxide dismutase on bleomycin-induced pulmonary fibrosis

Ken-Ichiro Tanaka,[1] Tomoaki Ishihara,[1] Arata Azuma,[2] Shoji Kudoh,[2] Masahito Ebina,[3] Toshihiro Nukiwa,[3] Yukihiko Sugiyama,[4] Yuichi Tasaka,[1] Takushi Namba,[1] Tsutomu Ishihara,[1] Keizo Sato,[1] Yutaka Mizushima,[5] and Tohru Mizushima[1]

[1]*Graduate School of Medical and Pharmaceutical Sciences, Kumamoto University, Kumamoto;* [2]*Department of Internal Medicine, Division of Respiratory, Infection, and Oncology, Nippon Medical School, Tokyo;* [3]*Department of Respiratory Medicine, Tohoku University Graduate School of Medicine, Sendai;* [4]*Department of Medicine, Jichi Medical University, Tochigi; and* [5]*DDS Institute, The Jikei University School of Medicine, Tokyo, Japan*

Submitted 20 August 2009; accepted in final form 21 December 2009

Tanaka K, Ishihara T, Azuma A, Kudoh S, Ebina M, Nukiwa T, Sugiyama Y, Tasaka Y, Namba T, Ishihara T, Sato K, Mizushima Y, Mizushima T. Therapeutic effect of lecithinized superoxide dismutase on bleomycin-induced pulmonary fibrosis. *Am J Physiol Lung Cell Mol Physiol* 298: L348–L360, 2010. First published December 24, 2009; doi:10.1152/ajplung.00289.2009.—Idiopathic pulmonary fibrosis (IPF) is thought to involve inflammatory infiltration of leukocytes, lung injury induced by reactive oxygen species (ROS), in particular superoxide anion, and fibrosis (collagen deposition). No treatment has been shown to improve definitively the prognosis for IPF patients. Superoxide dismutase (SOD) catalyzes the dismutation of superoxide anion to hydrogen peroxide, which is subsequently detoxified by catalase. Lecithinized SOD (PC-SOD) has overcome clinical limitations of SOD, including low tissue affinity and low stability in plasma. In this study, we examined the effect of PC-SOD on bleomycin-induced pulmonary fibrosis. Severity of the bleomycin-induced fibrosis in mice was assessed by various methods, including determination of hydroxyproline levels in lung tissue. Intravenous administration of PC-SOD suppressed the bleomycin-induced increase in the number of leukocytes in bronchoalveolar lavage fluid. Bleomycin-induced collagen deposition and increased hydroxyproline levels in the lung were also suppressed in animals treated with PC-SOD, suggesting that PC-SOD suppresses bleomycin-induced pulmonary fibrosis. The dose-response profile of PC-SOD was bell-shaped, but concurrent administration of catalase restored the ameliorative effect at high doses of PC-SOD. Intratracheal administration or inhalation of PC-SOD also attenuated the bleomycin-induced inflammatory response and fibrosis. The bell-shaped dose-response profile of PC-SOD was not observed for these routes of administration. We consider that, compared with intravenous administration, inhalation of PC-SOD may be a more therapeutically beneficial route of administration due to the higher safety and quality of life of the patient treated with this drug.

idiopathic pulmonary fibrosis; reactive oxygen species

IDIOPATHIC PULMONARY FIBROSIS (IPF) is a progressive and devastating chronic lung condition with poor prognosis; the mean length of survival from the time of diagnosis is 2.8–4.2 years. IPF progresses insidiously and slowly, and acute exacerbation of IPF is a highly lethal clinical event (1, 4, 21, 36). Current agents for the treatment of IPF, such as steroids and immunosuppressors, have not been found to improve the prognosis (1, 2, 26, 47), thus requiring the development of new types of drugs to treat IPF. To evaluate candidate drugs, the bleomycin-induced pulmonary fibrosis animal model provides a convenient option for the study (33).

Although the etiology of IPF is not yet fully understood, recent studies have suggested that it is triggered by lung injury and inflammation [infiltration of leukocytes (such as alveolar macrophages, lymphocytes, and neutrophils) and activation of cytokines]. Reactive oxygen species (ROS) that are released from the activated leukocytes cause further lung injury and inflammation. On the other hand, ROS and activated cytokines, especially TGF-β1, stimulate abnormal fibrosis (abnormal wound repair and remodeling) that is characterized by collagen deposition (22, 40). TGF-β1 seems to stimulate the production of interstitial collagen through both activation of fibroblasts and transformation of epithelial cells to fibroblasts (epithelial-mesenchymal transition; EMT) (3, 6, 48). This abnormal process of fibrosis is responsible for the pulmonary dysfunction associated with IPF. Supporting this idea, genetic inhibition of neutrophil elastase, of the TGF-β1-dependent signal transduction pathway, or of collagen synthesis was reported to suppress the progress of bleomycin-induced pulmonary fibrosis (5, 9, 14, 52). However, it is not clear whether pharmacological inhibition of these factors can improve the prognosis for IPF in humans.

A number of previous studies have suggested that the cellular redox state, determined by the balance between ROS (such as the superoxide anion) and antioxidant molecules [such as superoxide dismutase (SOD) and glutathione], plays an important role in the pathogenesis of IPF. Pulmonary inflammatory cells prepared from IPF patients generated higher levels of ROS than those from controls (25, 45). An increase in the level of ROS was reported in pulmonary tissues, blood, and bronchoalveolar lavage fluid (BALF) of IPF patients and bleomycin-administered animals (8, 18, 38, 41). Genetic modulation that increases or decreases the pulmonary level of ROS resulted in stimulation or suppression, respectively, of bleomycin-induced pulmonary fibrosis (11, 29). Thus, antioxidant molecules have attracted considerable attention as therapeutic candidates for the treatment of IPF. In fact, administration of *N*-acetylcysteine (NAC), which stimulates the synthesis of glutathione, exhibited therapeutic effects on IPF patients and bleomycin-induced pulmonary fibrosis in animals (10, 30, 31, 39).

SOD catalyzes the dismutation of superoxide anion to hydrogen peroxide, which is subsequently detoxified to oxygen and water by catalase or glutathione peroxidase (23). A decreased level of SOD was observed both in IPF patients and in

Address for reprint requests and other correspondence: T. Mizushima, Graduate School of Medical and Pharmaceutical Sciences, Kumamoto Univ., 5-1 Oe-honmachi, Kumamoto 862-0973, Japan (e-mail: mizu@gpo.kumamoto-u.ac.jp).

animals with bleomycin-induced pulmonary fibrosis (37, 53), thus suggesting that increasing SOD could be of therapeutic benefit in the treatment of IPF. However, the low affinity of SOD to the cell membrane where superoxide anion is produced, and its low stability in plasma, with a half-life of only a few minutes, were obstacles to the application of SOD in a clinical setting (13, 16, 17, 46). As a result of this, various SOD drug delivery systems have been devised to help overcome these limitations (16, 17, 20, 51).

Among these applications, lecithinized SOD (PC-SOD) has potentially beneficial effects for the treatment of IPF. PC-SOD is lecithinized human Cu/Zn-SOD in which four phosphatidylcholine (PC) derivative molecules are covalently bound to each SOD dimer (17). In vitro experiments with cultured cells have shown that this modification drastically improves the cell membrane affinity of SOD without decreasing its activity (16, 17), whereas in vivo experiments have demonstrated that it also greatly improves plasma stability (17). In a phase I clinical study, intravenously administered PC-SOD (40–160 mg) had a terminal half-life of more than 24 h, with good safety and tolerability (7, 42), and recently published results of a phase II clinical study have shown that intravenously administered PC-SOD (40 or 80 mg) significantly improved the symptoms of patients of ulcerative colitis (UC), which also involves ROS-induced tissue damage (43). Furthermore, intravenously administered PC-SOD ameliorated bleomycin-induced pulmonary fibrosis in mouse (44, 50), suggesting that PC-SOD could be effective in the treatment of IPF patients. However, a bell-shaped dose-response profile of PC-SOD has been reported for its ameliorative effect against bleomycin-induced pulmonary fibrosis (44, 50). Furthermore, when considering the quality of life (QOL) of patients, the present clinical protocol of PC-SOD administration (daily intravenous infusion for 4 wk) is expected to be improved. In this study, we provide evidence that the ineffectiveness of higher doses of PC-SOD is due to the accumulation of hydrogen peroxide. Furthermore, based on the results obtained here, we propose that administration of PC-SOD by inhalation is a clinically viable option to improve the QOL of IPF patients treated with this drug.

MATERIALS AND METHODS

Chemicals and animals. Paraformaldehyde, FBS, catalase from bovine liver (1,340 U/mg), an antibody against human Cu/Zn-SOD, 4-(dimethylamino)-benzaldehyde (DMBA), chloramine T, potassium dichromate, phosphotungstic acid, phosphomolybdic acid, Orange G, and acid fuchsin were obtained from Sigma (St. Louis, MO). Bleomycin was from Nippon Kayaku (Tokyo, Japan). Novo-heparin (5,000 units) for injection was from Mochida Pharmaceutical (Tokyo, Japan). Chloral hydrate was from Nacalai Tesque (Kyoto, Japan). Diff-Quik was from Sysmex (Kobe, Japan). Terminal deoxynucleotidyl transferase was obtained from Toyobo (Osaka, Japan). Biotin 14-ATP and Alexa Fluor 488 conjugated with streptavidin were purchased from Invitrogen (Carlsbad, CA). An ELISA kit for TGF-β1 was from R&D Systems (Minneapolis, MN). Mounting medium for immunohistochemical analysis (Vectashield) was from Vector Laboratories (Burlingame, CA). Cytospin 4 was purchased from Thermo Electron, whereas L-hydroxyproline, sodium acetate, TCA, azophloxin, and aniline blue were from Wako Pure Chemicals (Tokyo, Japan). Xylidine ponceau was from Waldeck (Muenster, Germany), and Mayer's hematoxylin, 1% eosin alcohol solution, mounting medium for histological examination (malinol), and Weigert's iron hematoxylin were from Muto Pure Chemicals (Tokyo, Japan). PC-SOD (3,000 U/mg) was from our laboratory stock (17). DAPI was from Dojindo (Kumamoto, Japan). Wild-type mice (6–8 wk old, ICR, male) were used. The experiments and procedures described here were carried out in accordance with the Guide for the Care and Use of Laboratory Animals as adopted and promulgated by the National Institutes of Health, and were approved by the Animal Care Committee of Kumamoto University.

Administration of bleomycin, PC-SOD, and catalase. ICR mice maintained under anesthesia with chloral hydrate (500 mg/kg) were given one intratracheal injection of bleomycin (5 mg/kg) in PBS (1 ml/kg) by use of micropipette (p200) to induce an inflammatory response and fibrosis. PC-SOD and catalase were dissolved in 5% xylitol and administered intravenously (tail vein) or intratracheally. For control mice, 5% xylitol solution was administered. The first administration of PC-SOD was performed just before the bleomycin administration.

For administration of PC-SOD by inhalation, five mice were placed in a chamber (volume, 45 l) and maintained under normoxic and normocapnic conditions. PC-SOD was dissolved in 10 ml of 5% xylitol, and an ultrasonic nebulizer (NE-U17 from Omron, Tokyo, Japan) that was connected to the chamber was used to nebulize the entire volume of the PC-SOD solution in 30 min. For control mice, 5% xylitol solution was subjected to nebulizer. Mice were kept in the chamber for a further 10 min after the 30 min of nebulizing.

Preparation of BALF and cell count. BALF was collected by cannulating the trachea and lavaging the lung with 1 ml of sterile PBS containing 50 U/ml heparin (two times). About 1.8 ml of BALF was routinely recovered from each animal. The total cell number was counted using a hemocytometer. Cells were stained with Diff-Quik reagents, and the ratios of alveolar macrophages, lymphocytes, and neutrophils to total cells were determined. More than 100 cells were counted for each sample.

Histological and immunohistochemical analyses and TUNEL assay. Lung tissue samples were fixed in 4% buffered paraformaldehyde and then embedded in paraffin before being cut into 4-μm-thick sections.

For histological examination, sections were stained first with Mayer's hematoxylin and then with 1% eosin alcohol solution. Samples were mounted with malinol and inspected with the aid of an Olympus BX51 microscope.

For staining of collagen (Masson's trichrome staining), sections were sequentially treated with *solution A* [5% (wt/vol) potassium dichromate and 5% (wt/vol) trichloroacetic acid], Weigert's iron hematoxylin, *solution B* [1.25% (wt/vol) phosphotungstic acid and 1.25% (wt/vol) phosphomolybdic acid], 0.75% (wt/vol) Orange G solution, *solution C* [0.12% (wt/vol) xylidine ponceau, 0.04% (wt/vol) acid fuchsin, and 0.02% (wt/vol) azophloxin], 2.5% (wt/vol) phosphotungstic acid, and finally aniline blue solution. Samples were mounted with malinol and inspected with the aid of an Olympus BX51 microscope.

For immunohistochemical analysis, sections were treated with 20 μg/ml·protease K for antigen activation and incubated with 0.3% hydrogen peroxide in methanol for removal of endogenous peroxidase. Sections were blocked with 2.5% goat serum for 10 min, incubated for 12 h with an antibody against human Cu/Zn-SOD (1:200 dilution) in the presence of 2.5% BSA, and then incubated for 1 h with peroxidase-labeled polymer conjugated to goat anti-mouse immunoglobulins. Then, 3, 3′-diaminobenzidine was applied to the sections, and the sections were finally incubated with Mayer's hematoxylin. Samples were mounted with malinol and inspected using a fluorescence microscope (Olympus BX51).

For the TUNEL assay, sections were incubated first with proteinase K (20 μg/ml) for 15 min at 37°C, then with TdTase and biotin 14-ATP for 1 h at 37°C, and finally with Alexa Fluor 488 conjugated with streptavidin and DAPI (5 μg/ml) for 2 h. Samples were mounted with Vectashield and inspected with the aid of a fluorescence microscope (Olympus BX51).

Hydroxyproline determination. Hydroxyproline content was determined as described (49). Briefly, the right lung was removed and homogenized in 0.5 ml of 5% TCA. After centrifugation, pellets were hydrolyzed in 0.5 ml of 10 N HCl for 16 h at 110°C. Each sample was incubated for 20 min at room temperature after addition of 0.5 ml of 1.4% (wt/vol) chloramine T solution and then incubated at 65°C for 10 min after addition of 0.5 ml of Ehrlich's reagent [1 M DMBA, 70% (vol/vol) isopropanol and 30% (vol/vol) perchloric acid]. Absorbance was measured at 550 nm, and the amount of hydroxyproline was determined.

Determination of the amount of PC-SOD, TGF-β1, and hydrogen peroxide in vivo. Determination of the amount of PC-SOD in serum and tissue was carried out as previously described (17). After administration of PC-SOD, the blood was collected, and serum samples were obtained by centrifugation. Furthermore, lungs were dissected, cut into small pieces, homogenized, and centrifuged to obtain the supernatants. The amount of PC-SOD in samples was determined using a human Cu/Zn-SOD ELISA kit (Bender MedSystem, Burlingame, CA). The amount of TGF-β1 in the lung tissue was also measured by ELISA according to the manufacturer's protocol.

For determination of hydrogen peroxide levels, lungs were dissected, cut into small pieces, suspended in PBS, and incubated for 30 min at 4°C with rotation. After centrifugation, the supernatants were applied to the NWLSS NWK-HYP01 assay kit (Northwest Life Science Specialties, Vancouver, WA).

Real-time RT-PCR analysis. Real-time RT-PCR was performed as previously described (32) with some modifications. Total RNA was extracted from pulmonary tissues using an RNeasy kit according to the manufacturer's protocol. Samples (2.5 μg RNA) were reverse-transcribed using a first-strand cDNA synthesis kit. Synthesized cDNA was used in real-time RT-PCR (Chromo 4 Instrument; Bio-Rad Laboratories, Hercules, CA) experiments using iQ SYBR GREEN Supermix and analyzed with Opticon Monitor Software. Specificity was confirmed by electrophoretic analysis of the reaction products and by inclusion of template- or reverse transcriptase-free controls. To normalize the amount of total RNA present in each reaction, actin cDNA was used as an internal standard.

Primers were designed using the Primer3 website. The primers used were (name: forward primer, reverse primer): *collagen type I*

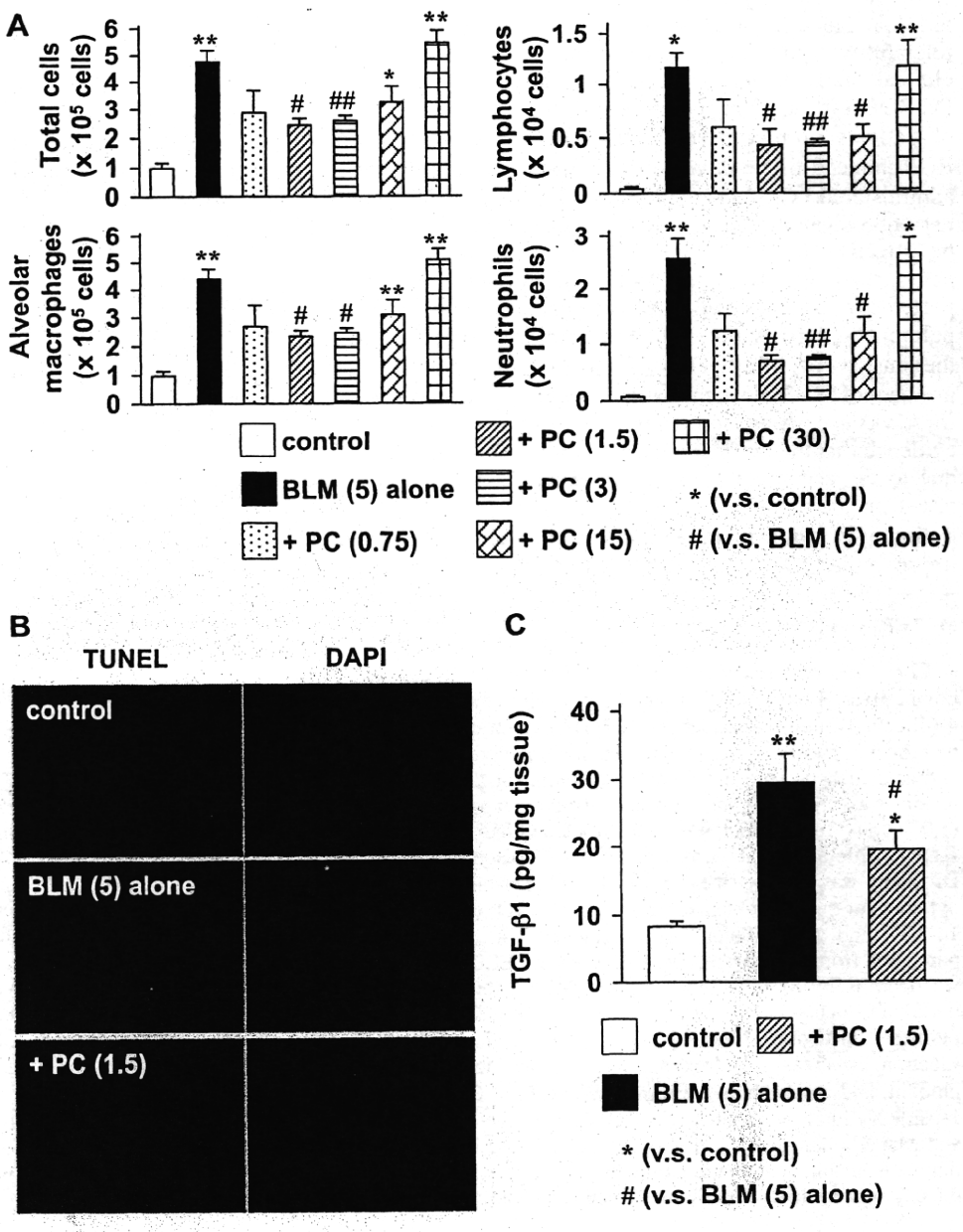

Fig. 1. Effect of intravenous administration of PC-SOD on bleomycin-induced inflammatory response. Mice treated with or without (vehicle) bleomycin (BLM) (5 mg/kg) once-only at *day 0* were intravenously administered indicated doses of PC-SOD (kU/kg) once per day for 3 days (*A–C*). Total cell number and numbers of alveolar macrophages, lymphocytes, and neutrophils were determined after 3 days as described in MATERIALS AND METHODS (*A*). Sections of pulmonary tissue were prepared after 3 days and subjected to TUNEL assay and DAPI staining. Similar results were obtained for at least 3 sections (*B*). The level of TGF-β1 in pulmonary tissue after 3 days was determined by ELISA (*C*). Values are means ± SE. * or #$P < 0.05$; ** or ##$P < 0.01$ (*A* and *C*).

(*Col1a1*): 5′-ccctgtctgcttcctgtaaact-3′, 5′-catgttcggttggtcaaagata-3′; *collagen type 3* (*Col1a3*): 5′-agggcagggaacaacttgatg-3′, 5′-ctccccttttgcacaaagctca-3′; *E-cadherin*: 5′-tgcccagaaaatgaaaaagg-3′, 5′-gtgtatgtggcaatgcgttc-3′; *Actin*: 5′-ggacttcgagcaagagatgg-3′, 5′- agcactgtgttggcgtacag-3′.

Statistical analysis. All values are expressed as means ± SE. Two-way ANOVA followed by the Tukey test or the Student's *t*-test for unpaired results was used to evaluate differences between more than three groups or between two groups, respectively. Differences were considered to be significant for values of $P < 0.05$.

RESULTS

Effect of PC-SOD on bleomycin-induced pulmonary fibrosis. Pulmonary fibrosis was induced in mice given a once-only (at *day 0*) intratracheal administration of bleomycin. The bleomycin-induced inflammatory response can be monitored as a function of the number of inflammatory cells (alveolar macrophages, lymphocytes, and neutrophils) in BALF 3 days after the administration of bleomycin. As shown in Fig. 1*A*, the total number of inflammatory cells and individual numbers of alveolar macrophages, lymphocytes, and neutrophils were all increased by the bleomycin treatment. This effect, however, could be suppressed by the simultaneous intravenous administration of PC-SOD, suggesting that PC-SOD ameliorates the bleomycin-induced pulmonary inflammatory response. PC-SOD produced a maximum beneficial effect at a dosage of 1.5–3 kU/kg, whereas a higher dose (30 kU/kg) did not suppress the bleomycin-induced pulmonary inflammatory response (bell-shaped dose-response profile) (Fig. 1*A*). Administration of the higher dose (30 kU/kg) of PC-SOD alone (without bleomycin administration) did not affect the number of inflammatory cells in BALF (data not shown).

Bleomycin-induced pulmonary fibrosis can be monitored by histopathological analysis and measurement of pulmonary hydroxyproline levels (an indicator of collagen levels) 14 days

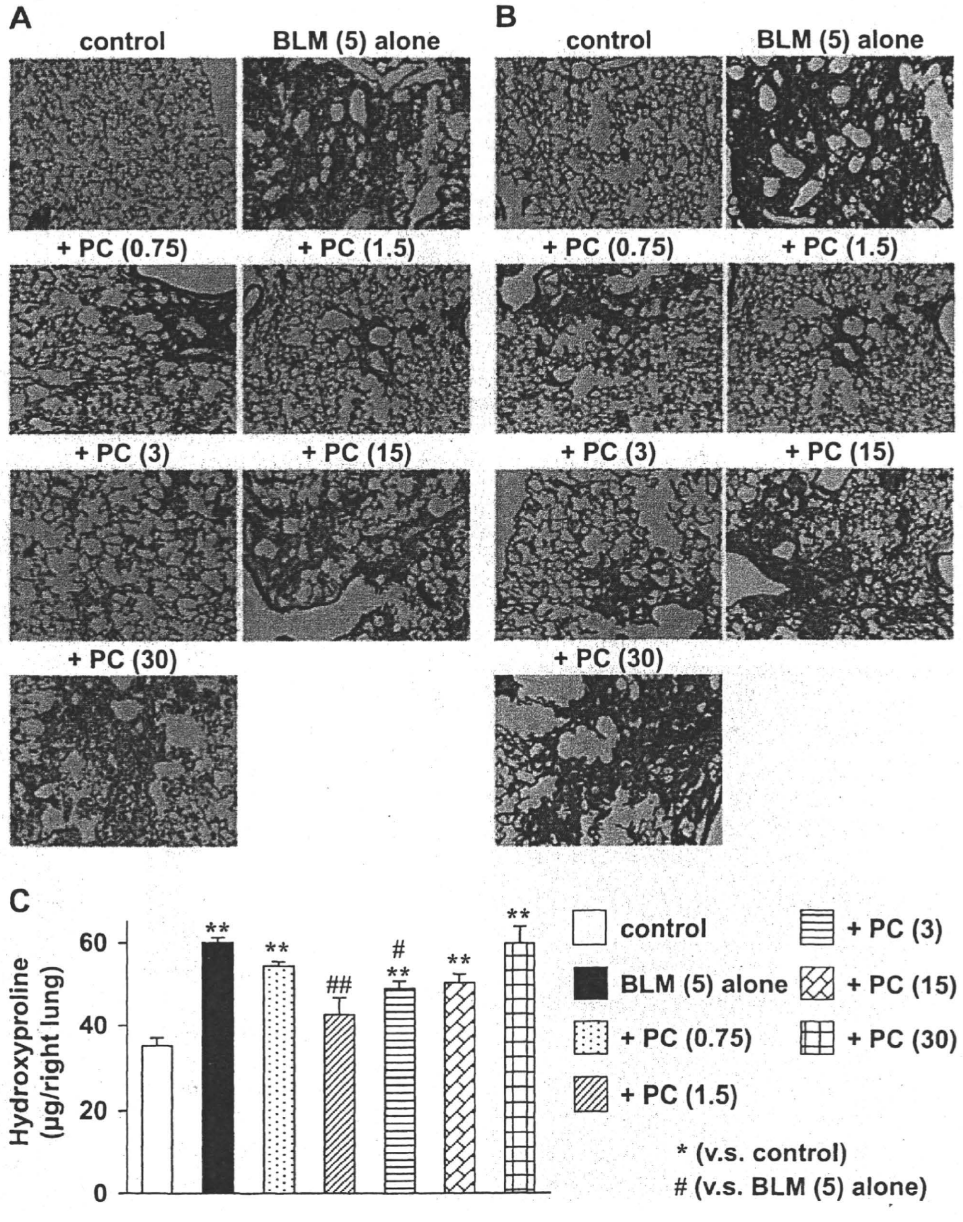

Fig. 2. Effect of intravenous administration of PC-SOD on bleomycin-induced pulmonary fibrosis. Mice treated once-only with or without (control) bleomycin (5 mg/kg) at *day 0* were intravenously administered indicated doses of PC-SOD (kU/kg) once per day for 14 days (*A–C*). Mice treated once-only with bleomycin (5 mg/kg) at *day 0* were intravenously administered indicated doses of PC-SOD (kU/kg) once per day from *day 7* to *day 13* (*D–F*). Sections of pulmonary tissue were prepared after 14 days and subjected to histopathological examination [H&E staining (*A* and *D*) or Masson's trichrome staining (*B* and *E*)] as described in MATERIALS AND METHODS. Similar results were obtained for at least 3 sections (*A*, *B*, *D*, *E*). The pulmonary hydroxyproline level was determined after 14 days as described in MATERIALS AND METHODS. Values are means ± SE. #$P <$ 0.05; ** or ##$P < 0.01$ (*C* and *F*).

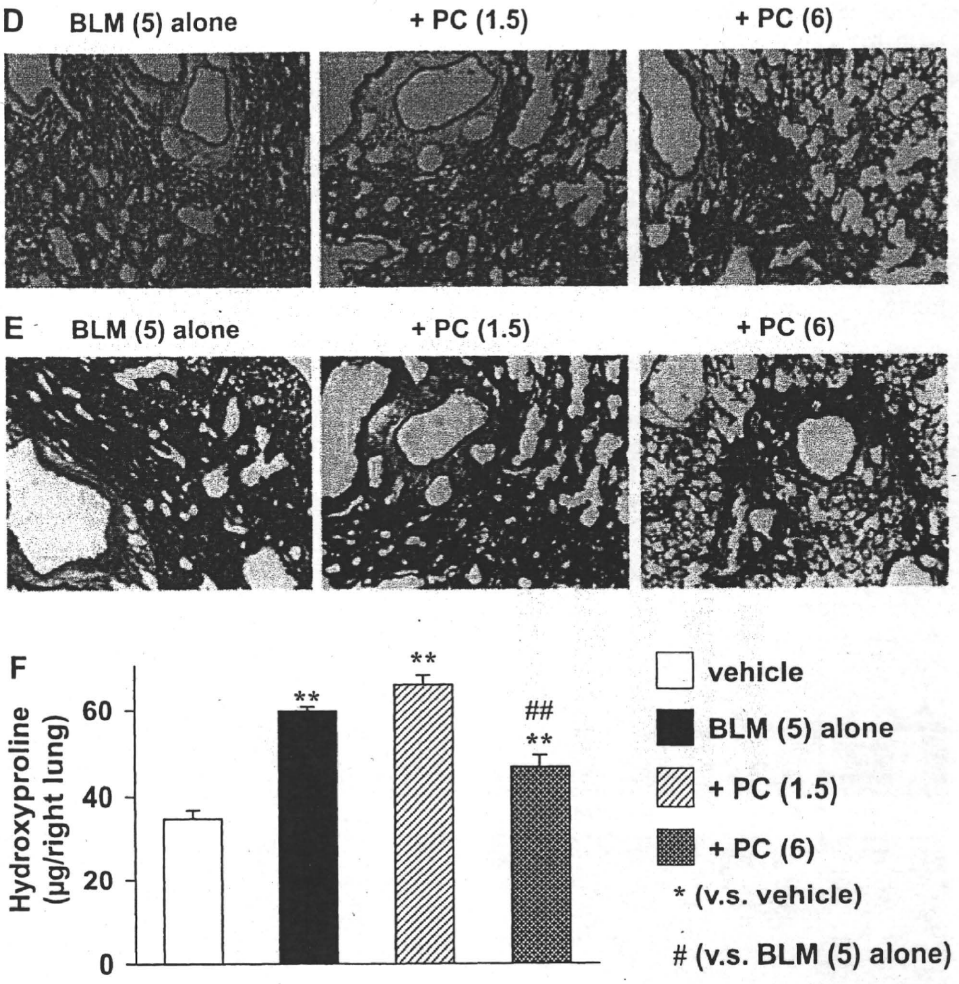

Fig. 2—*Continued*

after the administration of bleomycin. Histopathological analysis of pulmonary tissue using hematoxylin and eosin (H&E) staining revealed that the bleomycin administration induced severe pulmonary damage (thickened and edematous alveolar walls and interstitium) and infiltration of inflammatory cells into these regions (Fig. 2*A*). These phenomena were suppressed by the intravenous administration of PC-SOD (Fig. 2*A*). Again, a bell-shaped dose-response profile was observed; PC-SOD produced a maximum beneficial effect at 1.5–3 kU/kg, whereas at a higher dose (30 kU/kg) this ameliorative effect was not evident (Fig. 2*A*).

Masson's trichrome staining of collagen showed that bleomycin-induced collagen deposition was clearly suppressed by simultaneous intravenous administration of low doses (1.5–3.0 kU/kg) of PC-SOD, but not so clearly for a high dose (30 kU/kg) (Fig. 2*B*). As shown in Fig. 2*C*, a bell-shaped dose-response profile was also observed for the effect of PC-SOD on the bleomycin-induced elevation of pulmonary hydroxyproline content. The results in Fig. 2 thus support the fact that intravenous administration of PC-SOD ameliorates bleomycin-induced pulmonary fibrosis. We used an ELISA assay to determine the level of PC-SOD in serum and pulmonary tissue after its intravenous administration. As shown in Table 1, PC-SOD was detected in serum and pulmonary tissue 6 h after the final injection.

We also examined the effect of intravenous administration of PC-SOD on preexisting fibrosis; intravenous administration of PC-SOD was started at *day 7* after the administration of bleomycin. As shown in Fig. 2, *D–F*, bleomycin-induced

Table 1. *Serum and pulmonary levels of PC-SOD*

PC-SOD, Intravenous, kU/kg	*Plasma, U/ml*	*Lung, mU/mg Tissue*
0.75	7.80 ± 1.38	3.09 ± 0.84
1.5	16.9 ± 0.93	9.06 ± 1.29
15	128 ± 9.5	63.9 ± 1.86
30	245 ± 7.6	109 ± 4.3
PC-SOD, Intratracheal, kU/kg	*Plasma, U/ml*	*Lung, mU/mg Tissue*
0.15	n.d.	20.6 ± 10.5
0.75	0.30 ± 0.03	72.9 ± 5.31
1.5	0.75 ± 0.18	131 ± 28.6
15	5.34 ± 2.58	1,050 ± 381
30	12.5 ± 6.60	2,052 ± 702
60	26.6 ± 7.17	5,412 ± 183
PC-SOD, Inhalation, kU/Chamber	*Plasma, U/ml*	*Lung, mU/mg Tissue*
60	0.12 ± 0.06	22.7 ± 2.97
300	0.36 ± 0.12	51.9 ± 3.66
900	0.57 ± 0.12	198 ± 49.8

Mice treated with or without bleomycin (5 mg/kg) once-only at *day 0* were administered indicated doses of PC-SOD (kU/kg or kU/chamber) intravenously, intratracheally, or by inhalation once daily for 3 days. Blood and pulmonary tissue were taken 6 h after the final administration of PC-SOD. Levels of PC-SOD in samples were determined by ELISA. Values are means ± SE; n.d., not detected.

fibrosis was suppressed by a higher dose of PC-SOD (6 kU/kg) but not its low dose (1.5 kU/kg) under the conditions.

Mechanism for ameliorative effect of PC-SOD on bleomycin-induced pulmonary fibrosis. As described in the introduction, ROS-induced pulmonary cell death and TGF-β1-dependent stimulation of collagen synthesis and EMT play an important role in IPF and bleomycin-induced pulmonary fibrosis (24, 48). We examined effect of intravenous administration of PC-SOD on the extent of pulmonary cell death by employing the TUNEL assay. TUNEL-positive cells (indicative of cell death) increased in response to administration of bleomycin, and this increase was suppressed by simultaneous intravenous administration of PC-SOD (Fig. 1*B*), showing that PC-SOD protects pulmonary cells from cell death in vivo. We also examined the effect of PC-SOD on ROS-induced cell death in vitro, using A549 cells (human alveolar epithelial cell line). As shown in Fig. 3*A*, cell death induced by menadione, a superoxide anion-releasing drug, was inhibited by treatment of cells with PC-SOD.

A bleomycin-induced elevation of TGF-β1 levels in lung tissue was also suppressed by the intravenous administration of PC-SOD (Fig. 1*C*). We then examined effect of PC-SOD on the TGF-β1-dependent induction of collagen expression and EMT in vitro by using real-time RT-PCR analysis. Treatment of HFL-I cells (human embryonic lung fibroblast) with TGF-β1 induced the expression of *Col1a1* and *Col1a3* mRNA; the simultaneous treatment of cells with PC-SOD did not affect this induction (Fig. 3*B*). As shown in Fig. 3*C*, treatment of A549 cells with TGF-β1 induced or suppressed expression of *Col1a1* or *E-cadherin* mRNA, respectively, suggesting that

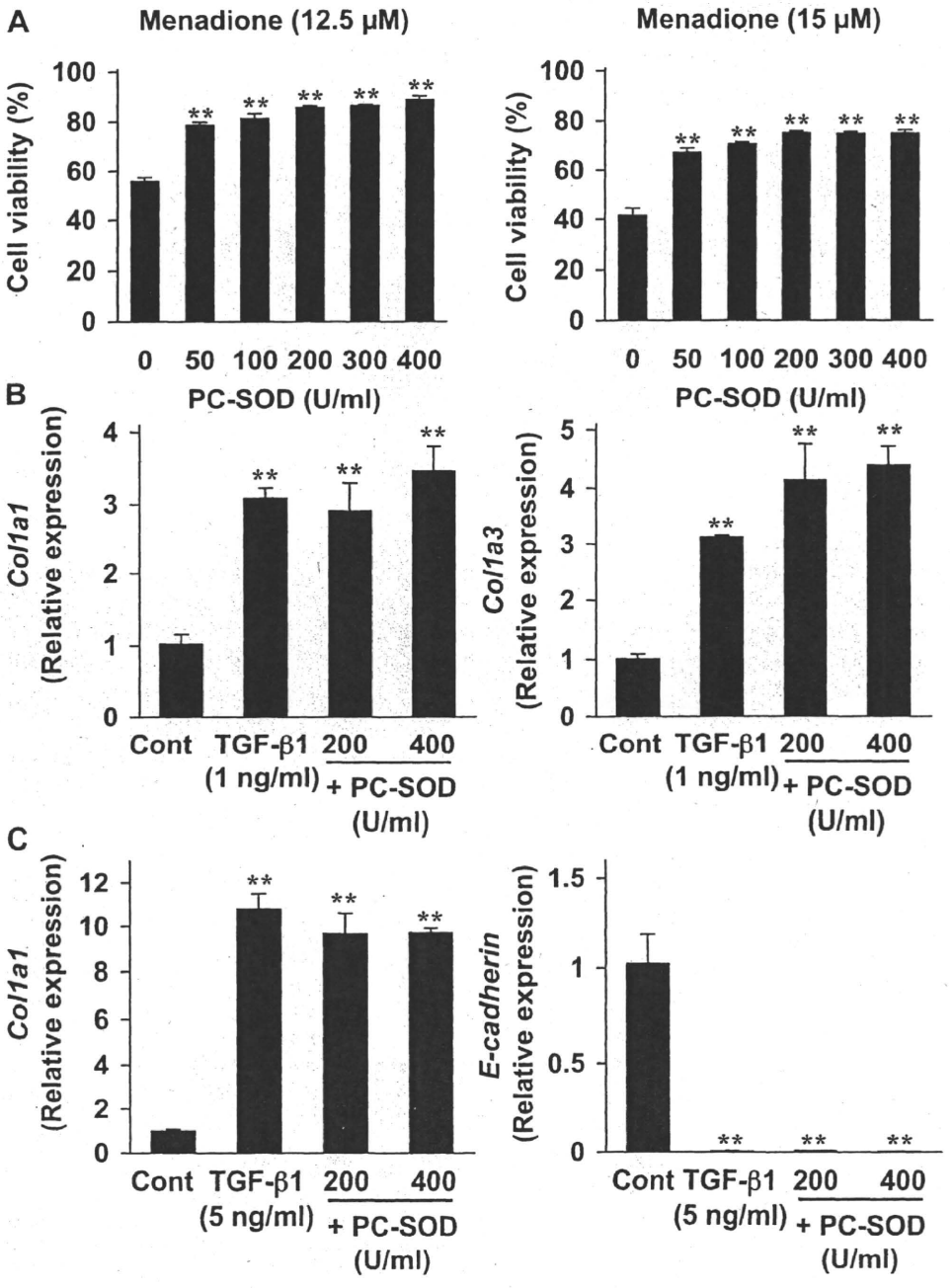

Fig. 3. Effect of PC-SOD on cell death and expression of collagen and epithelial-mesenchymal transition (EMT) in vitro. A549 (*A* and *C*) or HFL-I (*B*) cells were preincubated with the indicated concentration of PC-SOD for 1 h and further incubated with the indicated concentrations of menadione (*A*) or TGF-β1 (*B* and *C*) for 24 h in the presence of the same concentrations of PC-SOD as in the preincubation step. Cell viability was determined by MTT assay (*A*). Total RNA was extracted and subjected to real-time RT-PCR using a specific primer set for each gene. Values were normalized to the actin gene, expressed relative to the control sample (*B* and *C*). Values shown are means ± SE ($n = 3$). $^{**}P < 0.01$ (*A–C*).

EMT was induced. PC-SOD did not affect these TGF-β1-dependent alterations of mRNA expression (Fig. 3*C*). These results suggest that PC-SOD does not affect the TGF-β1-induced collagen synthesis and EMT.

Effect of simultaneous administration of catalase on the ameliorative effect of PC-SOD against bleomycin-induced pulmonary fibrosis. As described in the introduction, a bell-shaped dose-response profile of PC-SOD against bleomycin-induced pulmonary fibrosis has also been observed in other studies (44, 50). One possible explanation for the ineffectiveness of high doses of PC-SOD to combat the effects of bleomycin is the accumulation of hydrogen peroxide due to the relatively higher activity of SOD compared with catalase. We recently found evidence to support this notion in another animal model; simultaneous administration of catalase restored the ineffectiveness of higher doses of PC-SOD to combat dextran sulfate sodium-induced colitis, an animal model of UC (19). On this basis, we tested here the effect of concurrent administration of catalase on the activity of a high dose of PC-SOD in bleomycin-treated animals. Administration of 30 kU/kg PC-SOD improved the bleomycin-induced inflammatory response (increase in inflammatory cells in BALF) in the presence of the concurrent intravenous administration of catalase (1.5–6 kU/kg), but not in its absence (Fig. 4*A*). Administration of catalase alone did not significantly affect the bleomycin-induced inflammatory response (Fig. 4*A*).

We next examined the effect of simultaneous administration of catalase and high doses of PC-SOD on other aspects of bleomycin-induced pulmonary fibrosis. Bleomycin-induced pulmonary damage and infiltration of inflammatory cells into these regions were clearly suppressed by the simultaneous administration of catalase and a high dose of PC-SOD; however, treatment with either catalase or PC-SOD alone did not bring about such ameliorative effects (Fig. 4*B*). Collagen deposition and an increase in hydroxyproline levels were also clearly suppressed by the simultaneous

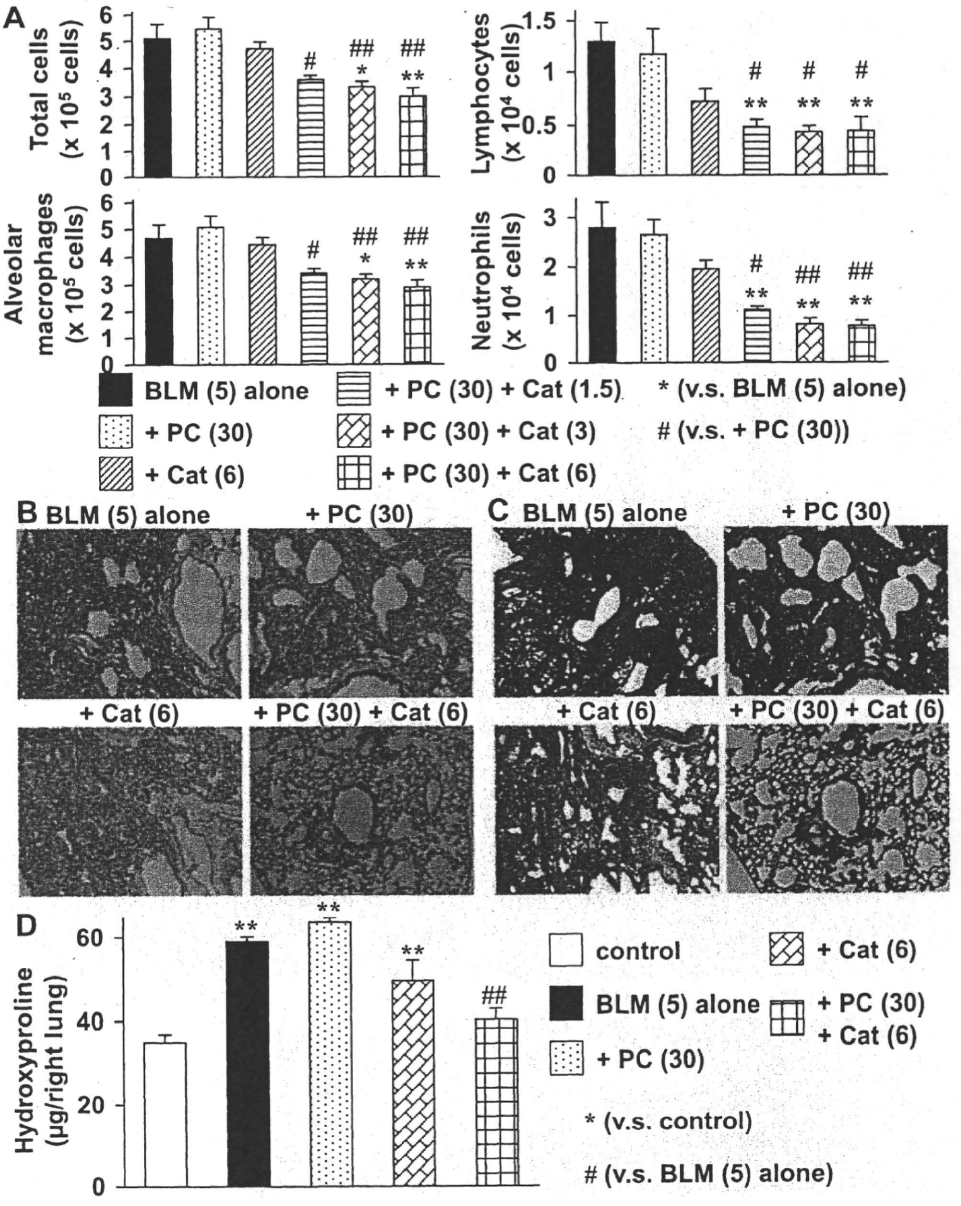

Fig. 4. Effect of concurrent administration of catalase on the ameliorative effect of PC-SOD on the bleomycin-induced inflammatory response and fibrosis. Mice were treated with bleomycin and PC-SOD, and the inflammatory response (*A*) and pulmonary fibrosis (*B–D*) were assessed as described in the legends of Figs. 1 and 2. The indicated dose of catalase (Cat) (kU/kg) was intravenously administered once per day for 3 days (*A*) or 14 days (*B–D*). Similar results were obtained for at least 3 sections (*B* and *C*). Values are means ± SE. * or #$P < 0.05$; ** or ##$P < 0.01$.

Table 2. *Effect of PC-SOD on pulmonary level of hydrogen peroxide*

PC-SOD, Intravenous, kU/kg	*Hydrogen Peroxide, μM*
Control	15.7 ± 0.81
1.5	17.4 ± 0.75
30	22.8 ± 1.33*
PC-SOD, Inhalation, kU/chamber	*Hydrogen Peroxide, μM*
Control	15.1 ± 1.79
60	13.1 ± 1.93
300	11.5 ± 0.95

Mice were administered indicated doses of PC-SOD (kU/kg or kU/chamber) intravenously or by inhalation once daily for 3 days. Lungs were removed, and the amount of hydrogen peroxide was determined. Values are means ± SE *$P < 0.01$; *vs. control.

administration of catalase and a high dose of PC-SOD (Fig. 4, *C* and *D*). Again, treatment with either catalase or a high dose of PC-SOD alone did not exert these beneficial effects (Fig. 4, *C* and *D*).

We further tested this idea by direct measurement of the pulmonary level of hydrogen peroxide. As shown in Table 2, administration of a high dose (30 kU/kg) but not a low dose (1.5 kU/kg) of PC-SOD increased the pulmonary level of hydrogen peroxide. The results shown in Fig. 4 and Table 2 suggest that the catalase-dependent restoration of efficacy of a high dose of PC-SOD on bleomycin-induced pulmonary fibrosis is due to the detoxification of hydrogen peroxide effects produced by a relatively higher activity of SOD.

Effect of modified methods of administration on PC-SOD's capacity to combat bleomycin-induced pulmonary fibrosis. To obtain some useful clues for refining the clinical guidelines for administration of PC-SOD, we tested the outcome of other routes of administration in the treatment of bleomycin-induced pulmonary fibrosis. As illustrated in Fig. 5*A*, the intratracheal administration of PC-SOD gave ameliorative effects against the bleomycin-induced inflammatory response. Interestingly, a bell-shaped dose-response profile was not observed with this

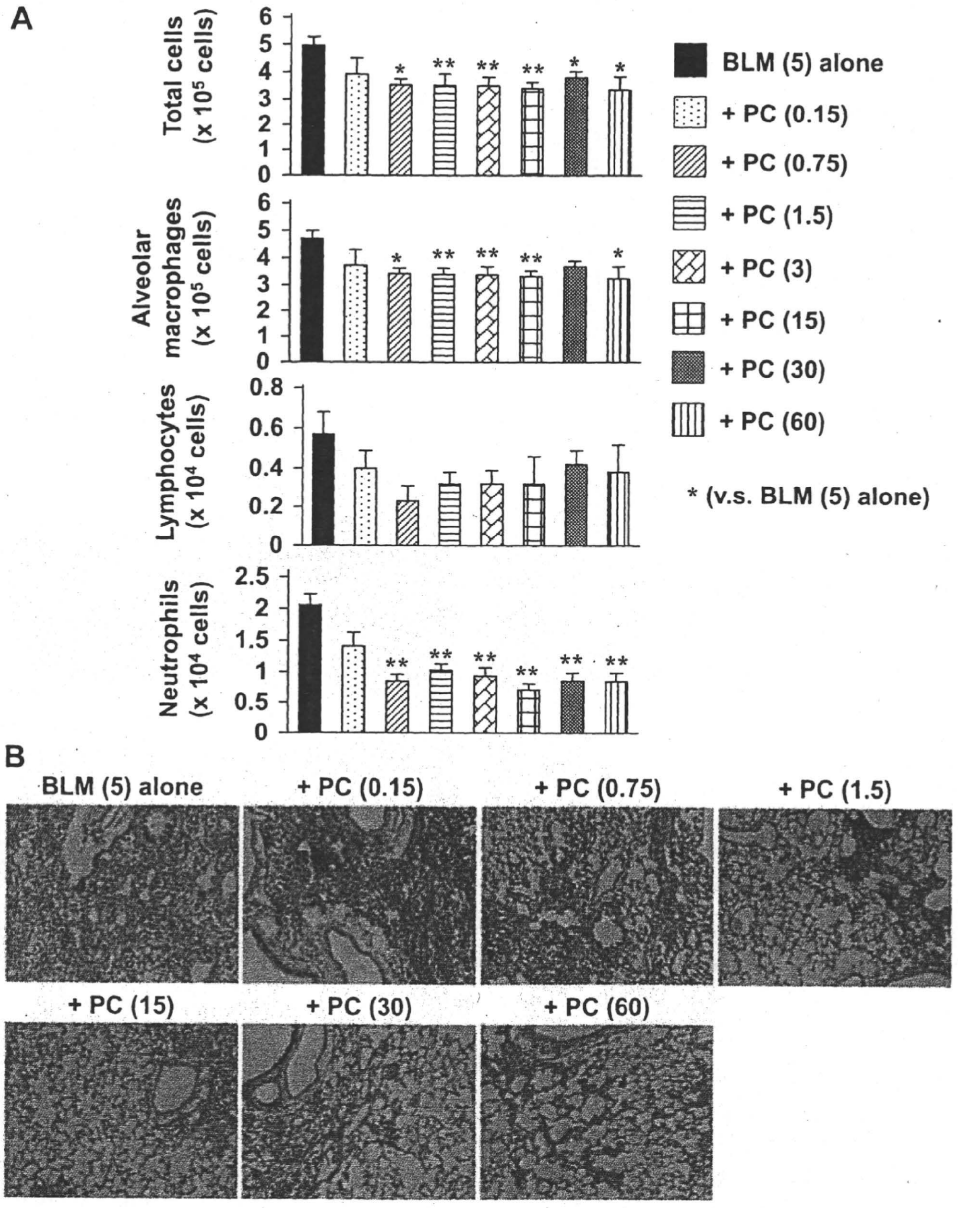

Fig. 5. Effect of intratracheal administration of PC-SOD on bleomycin-induced inflammatory response and pulmonary fibrosis. Mice were treated with bleomycin, and the inflammatory response (*A*) and pulmonary fibrosis (*B–D*) were assessed as described in the legends of Figs. 1 and 2. The indicated doses of PC-SOD (kU/kg) were administered intratracheally once per day for 3 days (*A*) or 14 days (*B–D*). Similar results were obtained for at least 3 sections (*B* and *C*). Values are means ± SE. * or #$P < 0.05$; ** or ##$P < 0.01$.